The Journal of Immunology

Crucial Contribution of Thymic Sirp{alpha}+ Conventional Dendritic Cells to Central Tolerance against Blood-Borne Antigens in a CCR2-Dependent Manner

Tomohisa Baba, Yasunari Nakamoto and Naofumi Mukaida

J. Immunol. 2009;183;3053-3063; originally published online Aug 12, 2009;
doi:10.4049/jimmunol.0900438
http://www.jimmunol.org/cgi/content/full/183/5/3053

The Journal of Immunology is published twice each month by The American Association of Immunologists, Inc., 9650 Rockville Pike, Bethesda, MD 20814-3994.

Print ISSN: 0022-1767 Online ISSN: 1550-6606.

Crucial Contribution of Thymic Sirpα^+ Conventional Dendritic Cells to Central Tolerance against Blood-Borne Antigens in a CCR2-Dependent Manner

Tomohisa Baba,* Yasunari Nakamoto,† and Naofumi Mukaida[1]*

Thymic dendritic cells (DCs) as well as thymic epithelial cells are presumed to be major sentinels in central tolerance by inducing the apoptosis of autoreactive T progenitor cells. The thymic DC population is composed of heterogeneous subsets including CD11c$^+$B220$^+$ plasmacytoid DCs, CD11c$^+$B220$^-$CD8α^+ signal regulatory protein α (Sirpα)$^-$ and CD11c$^+$B220$^-$CD8α^-Sirpα^+ conventional DCs (cDCs). However, the distinctive role of each DC subset remains undefined. We show herein that Sirpα^+ cDCs, a minor subpopulation, was disseminated in the thymic cortical area with some of them uniquely localized inside perivascular regions and nearby small vessels in the thymus. The Sirpα^+ but not Sirpα^- cDC subset can selectively capture blood-circulating Ags. Moreover, in CCR2-deficient mice, the thymic Sirpα^+ cDC subset, but not other thymic cell components, was moderately decreased especially in the perivascular regions. Concomitantly, these mice exhibited a modest impairment in intrathymic negative selection against blood-borne Ags, with the reduced capacity to uptake blood-borne Ags. Given their intrathymic cortical localization, CD11c$^+$B220$^-$CD8α^-Sirpα^+ cDCs can have a unique role in the development of central tolerance against circulating peripheral Ags, at least partially in a CCR2-dependent manner. *The Journal of Immunology,* **2009, 183: 3053–3063.**

The thymus is vital for development of T cells. T progenitor cells in the thymus are subjected to positive and negative selection, and survivors become self-MHC-restricted and self-tolerant mature naive T cells. Negative selection induces clonal deletion of potentially pathogenic autoreactive T cells and consequently decreases the risk of the development of autoimmune disorders (1). Thus, negative selection has a major role in central tolerance. Medullary thymic epithelial cells (mTECs)[2] are major inducers of negative selection. mTECs express the *autoimmune regulator (AIRE)* gene, which induces the ectopic expression of a milieu of peripheral tissue-specific Ags in the thymus resulting in the clonal deletion of autoreactive T progenitors with specificity for these Ags (2–4). Another type of thymic APCs, in particularly dendritic cells (DCs), have also been shown to contribute to negative selection (5–7). However, the detailed molecular and cellular mechanisms by which thymic DCs mediate negative selection remain largely unknown.

Thymic DCs are heterogeneous, similar to DCs in peripheral lymphoid organs such as lymph nodes and spleen. In humans and mice, thymic DCs are classified into two distinct subsets, CD11c$^+$B220$^+$ plasmacytoid DCs (pDCs) and CD11c$^+$B220$^-$ conventional DCs (cDCs). cDCs are further divided into CD11c$^+$CD11b$^-$CD8α^+Sirpα^- and CD11c$^+$CD11b$^+$CD8α^-Sirpα^+ subsets (8, 9). CD8α^+Sirpα^- cDCs, the most abundant subset among these three thymic DC subsets, are clustered in the medulla (10, 11). These CD8α^+Sirpα^- cDCs also express AIRE and can present endogenous self-Ags. In addition, they can cross-present tissue-specific Ags derived from the mTECs for negative selection (12, 13). In contrast, the intrathymic location and functions of another minor cDC, CD11c$^+$CD11b$^+$CD8α^-Sirpα^+, subset remain unclear, although this subset is presumed to migrate from the bloodstream (8). Proietto et al. (14) demonstrated that Sirpα^+ cDCs can induce thymocytes to efficiently differentiate into regulatory T cells in vitro. However, the roles of Sirpα^+ cDCs in central tolerance and regulatory T cell generation in vivo and the nature of the target autoantigens of central tolerance remain elusive.

Chemokines and their receptors have essential roles in controlling the homeostatic homing of immune cells including DCs and T cells (15–17). We examined the composition of thymic DC subsets in mice deficient in CCR1, CCR2, CCR5, or CX3CR1, the chemokine receptors which are expressed by DCs (18, 19). We observed that Sirpα^+ cDCs, but not Sirpα^- cDCs or pDCs, were selectively decreased in the thymus of CCR2-deficient mice, but not in the other chemokine receptor gene-deficient mice. Interestingly, CCR2-deficient mice exhibited a modest impairment in intrathymic negative selection against i.v. injected Ags. Concomitantly, CCR2 deficiency allowed releasing more autoreactive T cells against serum Ags into periphery. These Sirpα^+ cDCs migrated from bone marrow to thymus by the way of the peripheral blood and showed a unique intrathymic localization confined to perivascular and cortical areas. Moreover, Sirpα^+ cDCs had a greater capacity to uptake blood-borne Ags than Sirpα^- cDCs, along with their unique intrathymic localization. Thus, our present study suggests that thymic Sirpα^+ cDCs may function as a specialized APC for the development of central tolerance to blood-borne Ags.

*Division of Molecular Bioregulation, Cancer Research Institute and †Department of Disease Control and Homeostasis, Graduate School of Medical Science, Kanazawa University, Kanazawa, Ishikawa, Japan

Received for publication February 13, 2009. Accepted for publication June 8, 2009.

The costs of publication of this article were defrayed in part by the payment of page charges. This article must therefore be hereby marked *advertisement* in accordance with 18 U.S.C. Section 1734 solely to indicate this fact.

[1] Address correspondence and reprint requests to Dr. Naofumi Mukaida, Division of Molecular Bioregulation, Cancer Research Institute, Kanazawa University, 13-1 Takara-machi, Kanazawa 920-0934, Japan. E-mail address: naofumim@kenroku.kanazawa-u.ac.jp

[2] Abbreviations used in this paper: mTEC, medullary thymic epithelial cell; DC, dendritic cell; Sirpα, signal regulatory protein α; pDC, plasmacytoid DC; cDC, conventional DC; WT, wild type; Col IV, type IV collagen; FCM, flow cytometry; CMFDA, 5-chloromethylfluorescien diacetate; Cyt D, cytochalasin D; FSC, forward scatter; SSC, side scatter; DP, double positive.

www.jimmunol.org/cgi/doi/10.4049/jimmunol.0900438

Materials and Methods

Mice

Specific pathogen-free 6- to 7-wk-old male BALB/c mice were purchased from Charles River Japan and designated as wild-type (WT) mice. CCR1$^{-/-}$ and CX3CR1$^{-/-}$ mice were provided by Dr. P. M. Murphy (National Institute of Allergy and Infectious Diseases, National Institutes of Health, Bethesda, MD) (20, 21). CCR2$^{-/-}$ (22) and CCR5$^{-/-}$ mice (23) were provided by Dr. W. Kuziel (University of Texas San Antonio, San Antonio, TX) and Dr. Kouji Matsushima (University of Tokyo, Tokyo, Japan), respectively. All chemokine receptor-deficient mice were backcrossed to BALB/c mice for 8–10 generations. DO11.10 mice expressing a transgenic TCR that recognizes the $OVA_{323–339}$ peptide in the context of I-A^d were maintained as heterozygotes. DO11.10 mice were backcrossed to CCR2$^{-/-}$ mice to generate DO11.10/CCR2$^{-/-}$ mice. Genotyping for the *CCR2* gene was done by direct PCR from whole blood samples using an Ampdirect Plus kit (Shimadzu) and the specific primers (sense, 5′-CACGAAGTATCCAAGAGCTTG-3′ and antisense, 5′-CCCAAGTGAC TACACTTGTTA-3′). The mouse experiments were performed under specific pathogen-free conditions in accordance with the Guidelines for the Care and Use of Laboratory Animals of Kanazawa University.

Antibodies

Rat anti-mouse mAbs used were anti-CD3ε (145-2C11; Miltenyi Biotec), anti-CD4 (RM4-5; BD Pharmingen), anti-CD8 (53-6.7; BD Pharmingen), anti-CD25 (PC61; BD Pharmingen), anti-CD45R/B220 (RA3-6B2; BD Pharmingen), anti-CD172a/Sirpα (P84; BD Pharmingen), anti-DO11.10 clonotypic TCR (KJ1-26; BD Pharmingen), anti-F4/80 (A3-1; Serotec), and anti-Ly51 (6C3; BioLegend). Hamster anti-mouse CD11c (HL-3) and mouse anti-mouse I-A^d (AMS-32.1) mAbs were purchased from BD Pharmingen. Rabbit anti-mouse CCR2 mAb and anti-mouse type IV collagen (Col IV) polyclonal Ab were purchased from Epitomics and LSL, respectively. Goat anti-mouse MCP-2 polyclonal Ab was purchased from Santa Cruz Biotechnology. Isotype-matched control IgGs for each rat and hamster mAbs were purchased from BD Pharmingen. Mouse, rabbit, and goat IgG (Sigma-Aldrich) served as controls.

Cell preparation

Thymus was digested in 0.6 mg/ml collagenase type IV (Sigma-Aldrich) and 25 Kunitz units/ml DNase I (Sigma-Aldrich) in RPMI 1640 (Sigma-Aldrich) at 37°C for 20 min. The low-density cells were further isolated from the resultant single-cell suspensions using Histopaque-1077 reagent (Sigma-Aldrich). PBMCs were isolated from whole blood using Histopaque-1083 reagent (Sigma-Aldrich). Bone marrow cells were washed out with cold RPMI 1640 medium from the femoral and tibial bones.

Flow cytometry (FCM)

The low-density cells from thymus, PBMCs, and bone marrow cells were stained with various combinations of fluorescent dye-conjugated or nonconjugated specific Abs in PBS supplemented with 2 mM EDTA and 3% FBS. For nonconjugated Abs, fluorescent-conjugated secondary Abs were used. After washing in PBS, expression of cell surface molecular markers was analyzed using a FACSCalibur (BD Biosciences) with CellQuest Pro software (BD Biosciences).

Histology and fluorescent immunohistochemistry

Thymic tissues were frozen in OCT compound (Sakura) and 6-μm-thick cryostat sections were stained with H&E. For immunofluorescence analysis, 6-μm-thick cryostat sections were fixed with cold acetone for 3 min and incubated with Protein Block Reagent (DakoCytomation) to block nonspecific binding. Then fluorescent immunostaining was done by the standard method (for details, see the figure legends). After washing with 0.05% Tween 20-PBS, slides were mounted in fluorescent mounting medium (DakoCytomation). Immunofluorescence was detected in a setting that excluded the nonspecific signal of the isotype control using a fluorescence microscope (BX50; Olympus) or confocal laser-scanning microscope (LSM510; Zeiss). DP Controller software (Olympus) and Zen 2007 software (Zeiss) were used for image processing.

RT-PCR

Total RNAs were extracted from tissues using a RNeasy Mini Kit (Qiagen) and then reverse-transcribed using SuperScript III First-Strand Synthesis System (Invitrogen). PCR was done using the cDNAs, 2.5 mM dNTP mix (Takara), TaqDNA polymerase (Takara), and the specific primer sets for the *GAPDH* gene (sense, 5′-CAC TGA GCA TCT CCC TCA CA-3′ and antisense, 5′-TGG GTG CAG CGA ACT TTA TT-3′), *CD45* gene (sense, 5′-AAG ACA GAG TGC AAA GGA GAC-3′ and antisense, 5′-TGT AGG TGT TTG CCC TGT GAC AAA GAC-3′), *keratin 8* gene (sense, 5′-ACG GTG AAC CAG AGC CTG T-3′ and antisense, 5′-CTC CAC TTG GTC TCC AGC AT-3′), *MCP-1* gene (sense, 5′-CCC ACT CAC CTG CTG CTA CT-3′ and antisense, 5′-TCT GGA CCC ATT CCT TCT TG-3′), *MCP-2* gene (sense, 5′-CAG TCA CCT GCT GCT TTC AT-3′ and antisense, 5′-ATA CCC TGC TTG GTC TGG AA-3′), and *MCP-3* gene (sense, 5′-AAA CAA AAG ATC CCC AAG AGG-3′ and antisense, 5′-CAC AGA CTT CCA TGC CCT TC-3′) for 30 cycles of 95°C for 30 s, 55°C for 30 s, and 72°C for 30 s.

Effects of a peptide Ag on DO11.10 clonotypic thymocytes

DO11.10-transgenic mice with or without *CCR2* gene deficiency were administered 200 μg of $OVA_{323–339}$ peptide (ABGENT) in PBS through the tail vein. To induce thymocyte deletion independently of Ag presentation, mice were injected i.p. with 50 μg of anti-CD3ε mAb (24). Two days after injection, thymocytes were collected and stained with the following combinations of Abs: anti-CD4, anti-CD8, and anti-DO11.10 or anti-CD4, anti-CD25, and anti-DO11.10 Abs. To detect apoptotic cells, thymocytes were stained using an Annexin V-FITC Apoptosis Detection Kit (Merck). After being stained, the cells were analyzed by FCM.

Trafficking of bone marrow-derived immature DCs injected into bone marrow

Bone marrow cells were cultured in RPMI 1640 medium supplemented with 10% FBS and mouse GM-CSF (R&D Systems) at a concentration of 20 ng/ml. An equal volume of culture medium of the same content was added at 4 days, and one-half of the medium was replaced with fresh culture medium at 7 days after the plating. Most bone marrow cells were differentiated into immature DCs as judged by morphological appearances at 10 days after the initiation of the culture. The resultant immature DCs were stained with 1 μM 5-chloromethylfluorescein diacetate (CMFDA; Invitrogen) dye and 1 million cells were injected into the tibial bone marrow cavity of each mouse. After the injection, low-density cells were obtained from thymus, lymph nodes, or PBMCs to determine the presence of CMFDA-stained DCs by using FCM.

Localization of the i.v. injected Ags

Alexa Fluor 488-conjugated OVA protein (OVA_{488}), Alexa Fluor 647-conjugated OVA protein (OVA_{647}) (Invitrogen), or mouse serum IgG (Sigma-Aldrich), which was conjugated with Alexa Fluor 647, using an Alexa Fluor 647 protein labeling kit (Invitrogen), was injected into the tail vein of mice. Thymic low-density cells and PBMCs were isolated at the indicated time points after OVA protein injection and were stained with anti-CD11c and anti-Sirpα Abs. Then the cells were analyzed by FCM. For the localization of the Ag uptake, cryostat sections of frozen thymic tissues were obtained from mice injected with OVA protein and were stained with anti-Sirpα, anti-CD11c, anti-I-A^d, anti-Ly51, or anti-Col IV Abs and were then observed by fluorescence microscope.

In vitro endocytosis assay

Low-density cells were isolated from the thymus and were incubated with 10 μg/ml OVA_{647} in RPMI 1640 at 37°C for 20 min. As a negative control, incubation was conducted on ice. Endocytosis by each thymic DC subset was analyzed by FCM after being stained with anti-CD11c and anti-Sirpα Abs. In some experiments, low-density cells were preincubated with 10 μM cytochalasin D (Cyt D; Sigma-Aldrich), an actin inhibitor (25), 100 mM ammonium chloride (NH_4Cl) (Wako), an inhibitor of the clathrin-dependent pathway (26), or 0.5 mg/ml mannan (Sigma-Aldrich) at 37°C for 15 min before incubation with OVA_{647} at 37°C for 20 min in the presence of fresh inhibitors.

Adoptive transfer of bone marrow cells

Bone marrow cells were obtained from WT or CCR2$^{-/-}$ mice and were stained with 2 μM CMFDA dye. Twenty million cells were injected into the tail vein of CCR2$^{-/-}$ mice. OVA_{647} was injected into the tail vein at 2 days after injection. Thymic low-density cells were isolated at 1 h after OVA protein injection, and the presence of donor-derived Sirpα$^+$ cDCs and their capability of Ag uptake were analyzed by FCM.

In vivo cell proliferation assay

Spleen mononuclear cells were isolated from WT or CCR2$^{-/-}$ mice and were labeled with 25 μM CFSE using a CellTrace CFSE Cell Proliferation Kit (Invitrogen). Ten million prelabeled cells were injected into the tail vein of WT mice. One day after injection, mice were immunized with total

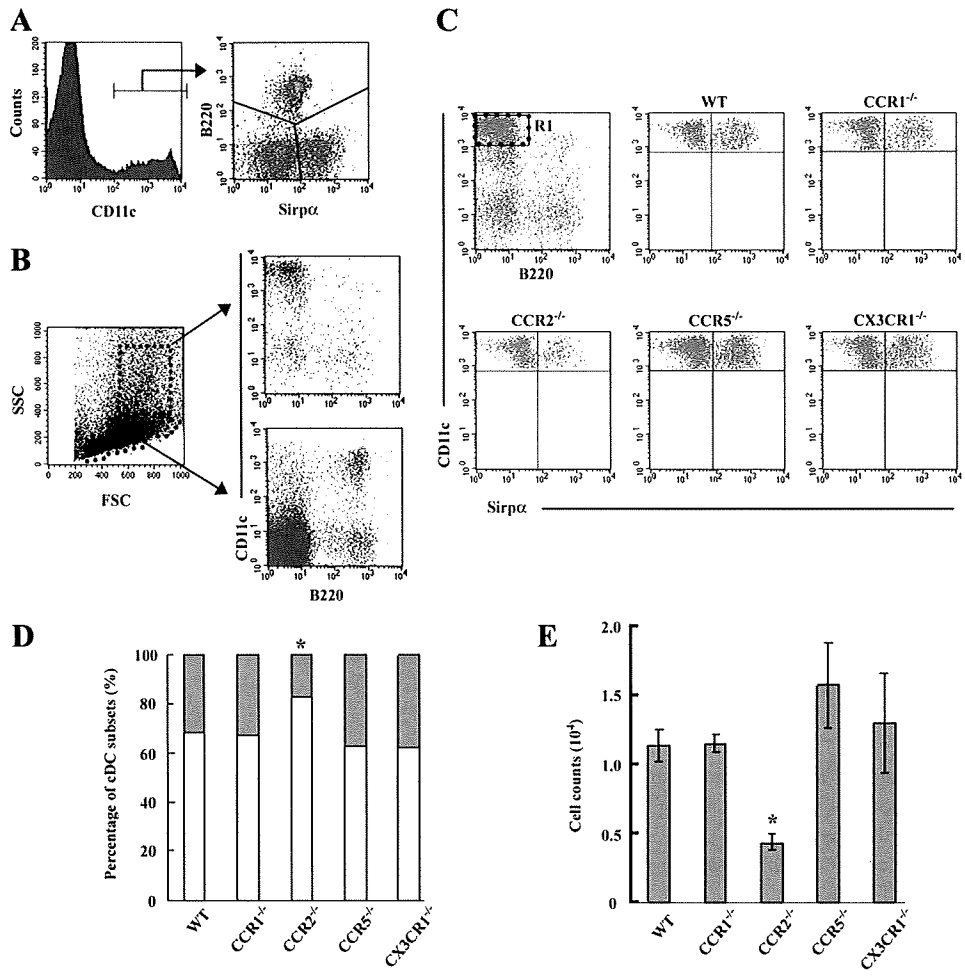

FIGURE 1. Effects of chemokine receptor deficiency on mouse thymic DC subsets. *A*, Low-density cells were isolated from WT mouse thymus and were stained with PE-conjugated anti-CD11c, allophycocyanin-conjugated anti-B220, and nonconjugated anti-Sirpα mAbs, followed by staining with FITC-conjugated mouse anti-rat IgG1. The CD11c$^+$ DC populations were gated to analyze the expression of Sirpα and B220. *B*, Thymic low-density cells were divided into two groups based on their FSC and SSC patterns, which are indicated by elliptic and square gates. Then DC subsets in each region were analyzed. *C*, Low-density cells were isolated from WT, CCR1$^{-/-}$, CCR2$^{-/-}$, CCR5$^{-/-}$, and CX3CR1$^{-/-}$ mice. The Sirpα$^-$ and Sirpα$^+$ subsets in FSC^{high} SSC^{high}CD11c^{high}B220$^-$ cDC populations gated with region 1 (R1) were compared among these mice. *D*, The ratio of two DC subsets (blank portion, Sirpα$^-$ subset; gray portion, Sirpα$^+$ subset) present in thymic cDC population was determined. Data represent the mean of three independent experiments. *E*, The numbers of Sirpα$^+$ DCs in the thymus. Data represent mean ± SD from three independent experiments. *, $p < 0.01$.

mouse serum protein emulsified in CFA. PBS in CFA was immunized as a control. Two days after immunization, lymphocytes were harvested from draining and nondraining lymph nodes and stained with anti-CD4 mAb. The percentage of CFSE-diluted divided cells was analyzed by FCM.

Statistical analysis

Data are represented as mean ± SD. Statistical significance was determined by one-way ANOVA followed by the Tukey-Kramer test. A value of $p < 0.05$ was considered statistically significant.

Results

Selective reduction of thymic Sirpα$^+$ cDCs in CCR2$^{-/-}$ mice

Consistent with a previous report (8), three distinct populations of thymic CD11c$^+$ DCs have been identified: B220$^+$ pDC, B220$^-$ Sirpα$^-$ cDC, and B220$^-$Sirpα$^+$ cDC subsets (Fig. 1*A*). cDC and pDC subsets were present mainly in the forward scatter (FSC^{high}), side scatter SSC^{high}, and SSC^{low} areas upon FCM, respectively (Fig. 1*B*). The pivotal role of chemokines in the trafficking of DCs prompted us to examine thymic DC subsets in mice deficient in chemokine receptor genes. Sirpα$^+$ DCs were markedly decreased in CCR2$^{-/-}$ mice, compared with WT mice, both in the relative (Fig. 1, *C* and *D*) and absolute number (Fig. 1*E*), whereas Sirpα$^-$ DC (Fig. 1*C*) and B220$^+$ pDC numbers (data not shown) were not changed in CCR2$^{-/-}$ mice. In contrast, no significant changes were observed on thymic cDC and pDC subsets in mice deficient in other chemokine receptors including CCR1, CCR5, and CX3CR1. Moreover, we did not observe any differences in thymic B220$^+$ B cell and F4/80$^+$ macrophage numbers between WT and CCR2$^{-/-}$ mice (data not shown). Microscopic studies of the thymus failed to reveal any morphological differences between WT and CCR2$^{-/-}$ mice in terms of the total cellularity, the distribution of thymocytes in each developmental stage, and the localization of Ly51$^+$ cortical thymic epithelial cells and I-A$^{d\ high}$ mTEC (supplemental Fig. S1[3]). Thus, CCR2$^{-/-}$ mice exhibit a selective decrease in the Sirpα$^+$ DC subset in thymus.

Attenuation of OVA$_{323-339}$ peptide-induced clonal deletion by CCR2 gene ablation

Sirpα$^+$ DCs are presumed to have the capacity to carry peripheral tissue Ags into the thymus (14). We next investigated the roles of Sirpα$^+$ DCs in thymus on taking in an i.v. administered Ag. PBS injection did not cause any changes in each developmental stage of thymocytes in DO11.10 and DO11.10/CCR2$^{-/-}$ mice (data not shown). On the contrary, i.v. administration of OVA$_{323-339}$ peptide markedly reduced the proportion and absolute number of clonotypic CD4/CD8 double-positive (DP) thymocytes in DO11.10 mice. *CCR2* gene ablation modestly attenuated this reduction (Fig. 2, *A–C*). OVA peptide injection consistently increased the proportion of annexin V$^+$ apoptotic cells in DO11.10 mouse thymus compared with that in DO11.10/CCR2$^{-/-}$ mice (Fig. 2*D*). In contrast, OVA peptide induced a modest increase in the number of DO11.10$^+$CD25$^+$CD4$^+$ regulatory T cell phenotype to similar extents in both DO11.10 and DO11.10/CCR2$^{-/-}$ thymus (Fig. 2*E*). Thus, decreased thymic Sirpα$^+$ DCs in CCR2$^{-/-}$ mice may be associated with a moderately impaired thymic negative selection. Moreover, following i.p. injection with anti-CD3 Ab (24), thymocytes were deleted to similar extents in DO11.10 and DO11.10/CCR2$^{-/-}$ mice

[3] The online version of this article contains supplemental material.

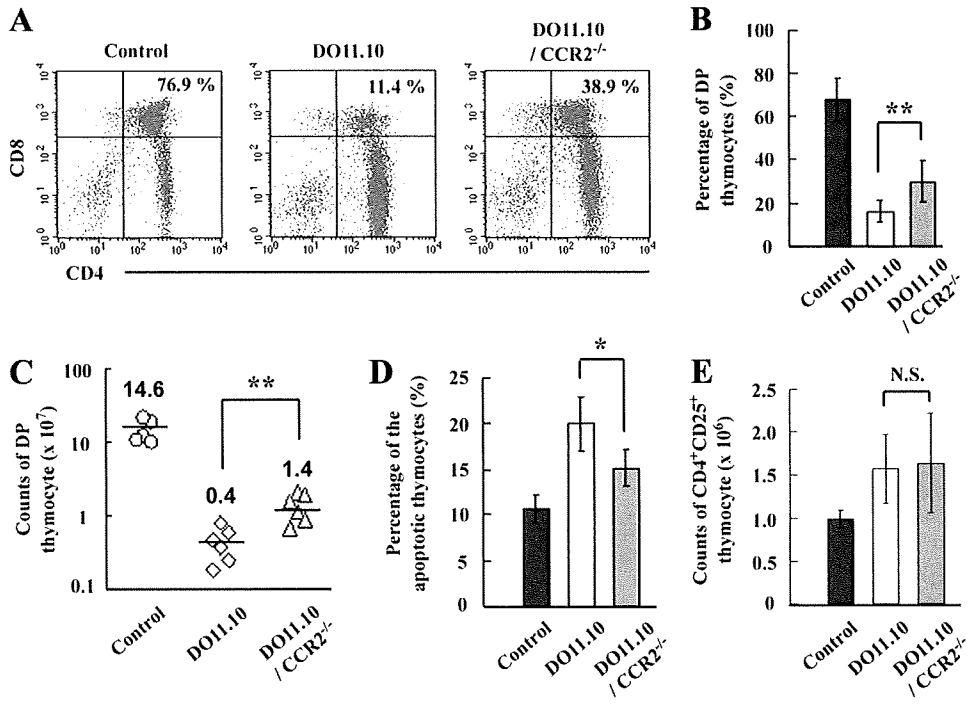

FIGURE 2. Induction of clonal deletion of DO11.10 clonotypic thymocytes. To induce the clonal deletion, 200 μg of $OVA_{323-339}$ peptide in PBS was injected into the tail vein of DO11.10-transgenic or DO11.10/$CCR2^{-/-}$ mice. PBS was injected as a control. DO11.10-transgenic TCR-expressing thymocytes were identified as KJ1-26-positive cells. *A*, Each developmental stage of thymocytes after $OVA_{323-339}$ peptide injection. Percentage of DP stage is shown in each panel. *B*, Percentage of DP stage of development; *C*, the number of DP thymocytes; *D*, percentage of the apoptotic thymocytes; and *E*, the number of $CD4^+$ $CD25^+$ thymocytes were determined on DO11.10 and DO11.10/$CCR2^{-/-}$ mice. Representative results from at least four independent experiments are shown in *A* while the mean ± SD was calculated on at least four independent experiments and are shown in *B–E*. *, $p < 0.05$ and **, $p < 0.01$. N.S., No significant difference.

(supplemental Fig. S2), indicating the absence of intrinsic defects of thymocytes in the absence of CCR2. These results collectively suggest that thymic Sirpα+ DCs can contribute to intrathymic negative selection of a bloodstream-derived Ag without inducing regulatory T cells.

Thymic Sirpα+ DCs can efficiently capture peripheral Ag from bloodstream

To elucidate the functions of thymic Sirpα+ DCs more in detail, we determined their intrathymic localization. In thymi of WT mice, Sirpα was mainly detected on $CD11c^+$ DCs scattered in the thymic cortex (Fig. 3, *A* and *B*), but not on $CD11c^+$ DCs clustered in medulla, the predominating site of thymic $CD8\alpha^+Sirp\alpha^-$ DCs. Moreover, most Sirpα+ DCs were localized in close proximity to small vessels with single Col IV^+ basement membrane or inside perivascular regions (PVRs) separated by two Col IV^+ basement membranes in the cortex (Fig. 3*C*). The thymic DC population includes APCs crucially involved in the central tolerance system involving bloodstream C5 Ag (27). Furthermore, Sirpα+ DCs are selectively localized in PVRs or in close proximity to small vessels, both essential components of the blood-thymus barrier (28). Hence, we hypothesized that this DC subset might be involved in Ag uptake from the bloodstream. To address this possibility, we treated WT mice i.v. with OVA_{647} and examined its uptake by thymic DCs. Intrathymic Sirpα+ DCs, but not Sirpα− DCs, took up OVA protein in a dose-dependent manner (Fig. 4*A*), maintaining a stable level from 1 to 4 h after the injection and decreasing thereafter (Fig. 4*B*). Recently, it was reported that bloodstream DCs could efficiently capture and transport particulate bacteria into the spleen when particulate bacteria were i.v. injected (29). Indeed, bloodstream $CD11c^+$ cells rapidly disappeared from the peripheral blood after capturing OVA protein (Fig. 4*C*). By contrast, the uptake by intrathymic Sirpα+ DCs reached a peak level at 15 min, decreasing to the stable level thereafter. Thus, there may be a remote possibility that circulating DCs migrated into the thymus after capturing OVA protein inside the bloodstream. Furthermore, in addition to an exogenous protein, intrathymic Sirpα+ DCs also captured an endogenous serum protein, mouse IgG, which was conjugated with Alexa Fluor 647, when it was administered i.v. (supplemental Fig. S3). Thus, Sirpα+ DCs can effectively capture peripheral Ags from the bloodstream across the blood-thymus barrier. This notion was further supported by the observation that Sirpα+ DCs engulfed OVA protein with a higher efficiency than Sirpα− DCs when cultured in vitro with OVA_{647} (Fig. 4, *D* and *E*). Mannan from *Saccharomyces cerevisiae*, but not NH_4Cl or Cyt D from *Zygosporium mansonii*, markedly inhibited endocytosis of OVA protein by Sirpα− DCs (Fig. 4*F*, *upper panel*). On the contrary, uptake of OVA protein by Sirpα+ DCs was markedly attenuated by NH_4Cl and Cyt D, but not mannan (Fig. 4*F*, *lower panel*). These observations suggest that thymic Sirpα+ DCs can endocytose soluble Ags more efficiently than Sirpα− DCs, in a clathrin-dependent, but not mannose receptor-dependent manner.

Thymic Sirpα+ DCs capture peripheral Ag inside PVRs or nearby small vessels, and then migrate into the cortical parenchyma

We examined sequentially intrathymic localization of OVA-derived signals after i.v. injection of OVA_{488}. By 0.5 h, OVA_{488}-derived signals were detected in Sirpα+ cells (Fig. 5*A*), $CD11c^+$ DCs (Fig. 5*B*) and inside PVRs or in close proximity to small vessels (Fig. 5*C*). Although some signals remained nearby in small vessels, signals inside PVRs were obviously decreased at 6 h (Fig. 5*D*), as judged by the Col IV immunostaining pattern. At 18 h after the injection, OVA_{488}-derived signals were mainly scattered in the $Ly51^+$ cortical area but not in the $I\text{-}A^{d\ high}$ medullary area (Fig. 5*E*). Because OVA_{488}-derived signals were constantly detected in Sirpα+ DCs at every time point (data not shown), these observations suggest that Sirpα+ DCs initially capture bloodstream OVA protein inside PVRs or in nearby small vessels and then migrate into the cortical parenchyma. To examine the process of migration more in detail, OVA_{647} (blue) and OVA_{488} (green) were i.v. injected sequentially with an interval of either 6 or 18 h as shown in Fig. 5*F*. When OVA_{488} was injected 6 h after OVA_{647}, double-positive $CD11c^{high}$ DCs were evidently detected (8.1%), while single-positive cells were sparse (Fig. 5*F*, *left upper panel*). Even at 18 h after the injection, double-positive $CD11c^{high}$ DCs were still

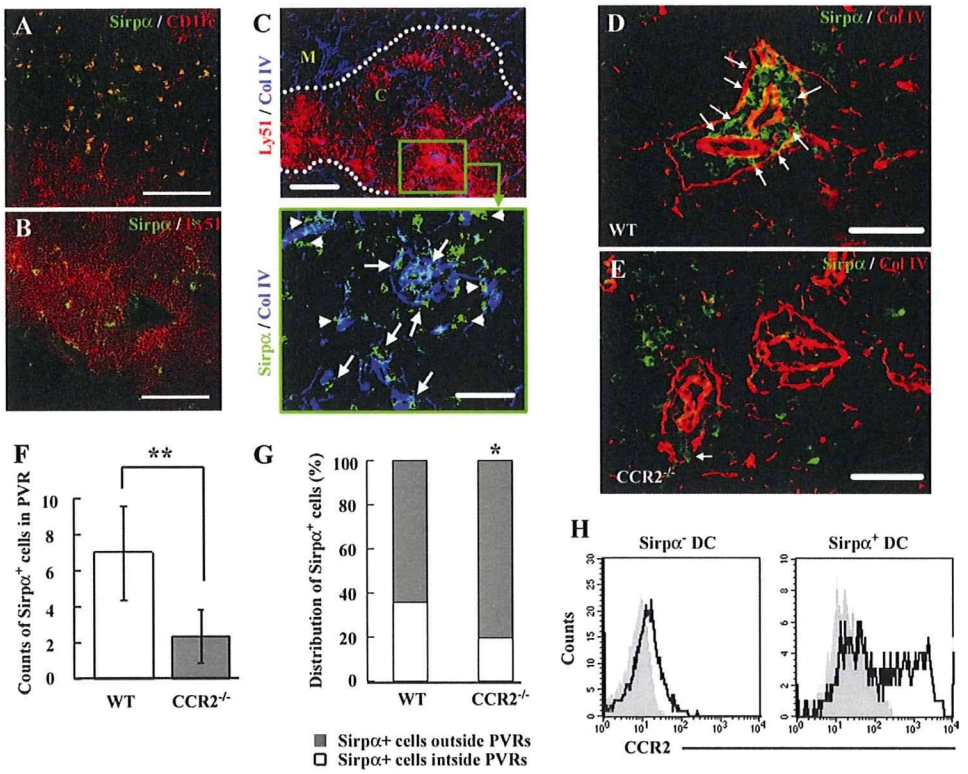

FIGURE 3. Localization of thymic Sirpα$^+$ DCs. Double-color fluorescence immunostaining for Sirpα (green) and CD11c (red; *A*), Ly51 (red; *B*), or Col IV (red; *D* and *E*). *C*, Triple-color fluorescent immunostaining for Sirpα (green), Ly51 (red), and Col IV (blue). Low magnification image for Ly51 and Col IV is shown in the *upper panel*. A green square in the *upper panel* is observed at a higher magnification for Col IV and Sirpα expression and is shown in the *lower panel*. Dashed lines indicate the boundary between cortex (C) and medulla (M). Arrowheads in *C* and arrows in *C–E* indicate Sirpα$^+$ cells interacting with small vessels and inside the PVRs, respectively. *A–D*, WT thymus. *E*, CCR2$^{-/-}$ thymus. Representative results from at least two independent experiments are shown here. Scale bars: *A* and *B*, 100 μm; *upper panel* of *C*, 200 μm; *lower panel* of *C–E*, 50 μm. *F* and *G*, At least five photographs in the central regions of the PVRs were taken at ×200 magnification in each tissue sample. The numbers of Sirpα$^+$ cells inside the PVRs were determined and data represent mean ± SD of three independent experiments. **, $p < 0.01$. *F*, The proportion of Sirpα$^+$ cells inside the PVRs to outside was calculated and data represent the mean of three independent experiments. *, $p < 0.05$ (*G*). *H*, CCR2 expression on CD11c^{high}Sirpα$^-$ or Sirpα$^+$ cDCs. Gray-filled and black-open histograms indicate the results from isotype control and specific mAb for CCR2, respectively. Representative results from three independent experiments are shown here.

present (3.2%) with substantial numbers of OVA_{488}-derived signal single-positive (3.9%) or OVA_{647}-derived signal single-positive cells (2.3%; Fig. 5*F*, *left lower panel*). Thus, CD11c^{high} DCs with Sirpα expression can persistently be in close interaction with the bloodstream while they are migrating into cortical parenchyma (Fig. 5*G*).

Depressed migration of Sirpα$^+$ DCs and their aberrant intrathymic localization in CCR2$^{-/-}$ mice

It is possible that a decreased intrathymic Sirpα$^+$ DC number may account for the defect in their migration in CCR2$^{-/-}$ mice, because the thymic Sirpα$^+$ cDC subset is presumed to migrate from the bloodstream (14). Most CD11c$^+$B220$^-$ DCs in peripheral blood and bone marrow expressed abundantly Sirpα (supplemental Fig. S4), similarly as observed on thymic Sirpα$^+$ DCs, and this population expressed CCR2 (supplemental Fig. S5). CCR2$^{-/-}$ mice exhibited a moderate reduction in CD11c$^+$B220$^-$ DCs in peripheral blood, but not bone marrow (Fig. 6, *A* and *B*). This suggests a possible defect in the migration of CD11c$^+$B220$^-$ DCs from bone marrow in CCR2$^{-/-}$ mice. To test this possibility, bone marrow cells were induced to differentiate to DCs with in vitro GM-CSF stimulation, labeled with CMFDA, and injected into bone marrow of WT mice (Fig. 6*C*, *upper illustration*). Under these conditions, >80% of injected cells expressed CD11c, Sirpα, and CCR2, but not B220 (supplemental Figs. S4 and S5). WT-derived DCs appeared in peripheral blood rapidly within 2 h after the intra-bone marrow injection, whereas CCR2$^{-/-}$ mouse-derived DCs migrated into peripheral blood less efficiently (Fig. 6, *C* and *D*). Interestingly, CD11c$^+$B220$^-$Sirpα$^+$ DCs appeared in thymus by 6 h after intra-bone marrow injection (Fig. 6*E*). These observations suggest that CCR2-mediated signals were critical of the migration of Sirpα$^+$ DCs from bone marrow into the thymus. Moreover, Sirpα$^+$ DCs were markedly decreased in PVRs of CCR2$^{-/-}$ thymus compared with those of WT thymus (WT mice, 7.0 ± 2.6/site; CCR2$^{-/-}$ mice, 2.3 ± 1.5/site; Fig. 3, *D–F*). Furthermore, the decrease was more evident in the region inside the PVRs compared with that outside the PVRs (Fig. 3*G*). CCR2 was expressed also by a portion of intrathymic Sirpα$^+$ DCs, but not Sirpα$^-$ DCs (Fig. 3*H*). Three mouse chemokines, MCP-1, MCP-2, and MCP-3, can bind to CCR2 (30). Among these chemokines, only MCP-2 mRNA was constitutively expressed in thymus, particularly keratin 8-positive thymic stroma, but not CD45-positive thymocytes (Fig. 7, *A* and *B*). Moreover, MCP-2 immunoreactivities were consistently detected inside the PVRs (Fig. 7*C*, *upper panels*) and on Sirpα$^+$ cells in the PVRs (Fig. 7*C*, *lower panels*). Thus, it is probable that the CCR2-MCP-2 interaction can contribute to intrathymic localization of Sirpα$^+$ DCs, particularly in the PVRs.

Defective Ag uptake by Sirpα$^+$ DCs in CCR2$^{-/-}$ mice

Because the PVR was proved to be a main location of the uptake of circulating Ags, we further examined the effects of CCR2

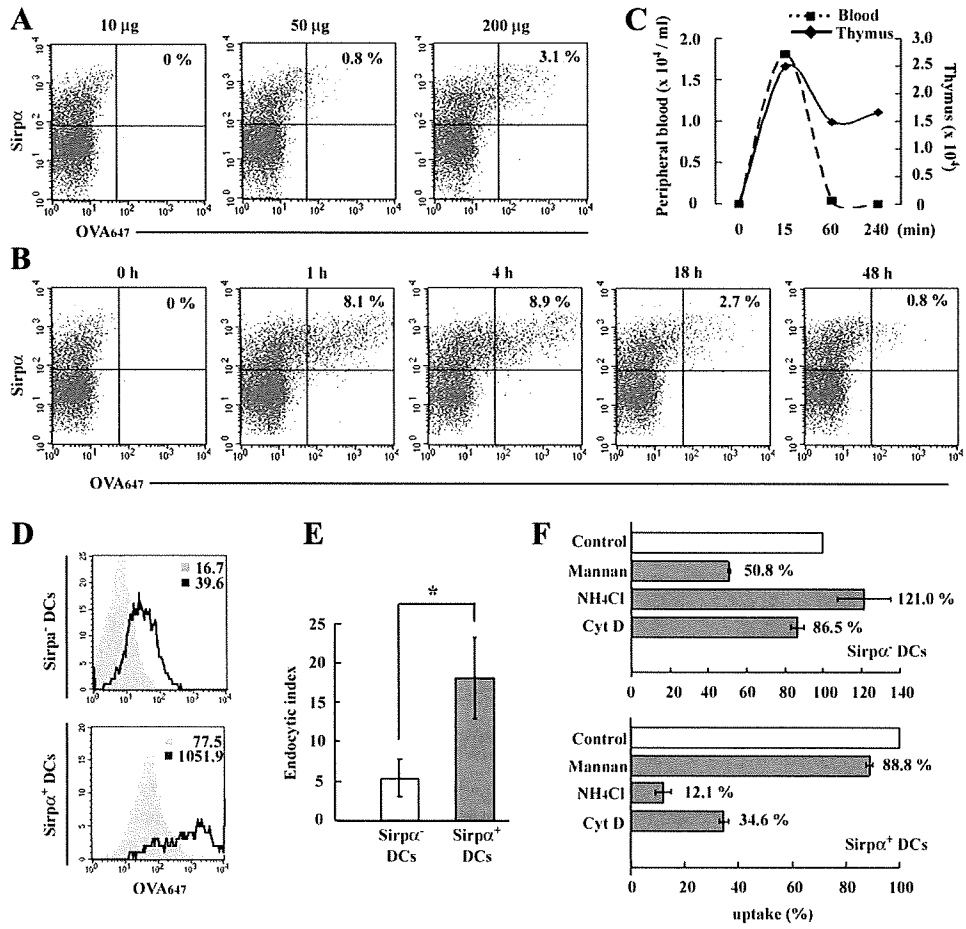

FIGURE 4. Uptake of bloodstream Ag by thymic Sirpα$^+$ DCs. *A*, At 18 h after injection with OVA_{647} at the indicated doses, low-density cells were isolated from WT thymus and were stained with anti-CD11c and anti-Sirpα mAbs. Then the uptake of OVA_{647} in the $CD11c^{high}$ DC population was analyzed. *B*, Uptake of OVA_{647} at the indicated time points. OVA_{647} (200 μg) was injected into the tail vein. Percentage of Sirpα$^+OVA_{647}^+$ region is shown in each panel of *A* and *B*. Representative results from three independent experiments are shown. *C*, Time kinetics of the numbers of DCs capturing OVA protein in the peripheral blood (broken line) and thymus (solid line). *D*, In vitro endocytosis of OVA_{647} by $CD11c^{high}$Sirpα$^-$ and $CD11c^{high}$Sirpα$^+$ cDCs are shown in the *upper* and *lower panels*, respectively. Gray-filled and black-open histograms indicate the results obtained when the cells were incubated at 0 and 37°C, respectively. Numbers in each panel indicates mean fluorescence intensity for OVA_{647} captured. Representative results from three independent experiments are shown here. *E*, Endocytic index in Sirpα$^-$ and Sirpα$^+$ cDCs. Endocytic index was calculated as mean fluorescence intensity at 37°C/mean fluorescence intensity at 0°C. Mean ± SD were calculated from three independent experiments and are shown here. *, $p < 0.01$. *F*, The effects of various agents on endocytosis. Uptake in the presence of each inhibitor is shown as the percentage of total uptake in the absence of any inhibitors. Means were calculated from three independent experiments and are shown here.

deficiency on the capability of Sirpα$^+$ DCs to uptake Ags from the bloodstream. Indeed, when OVA_{647} was injected i.v., $CCR2^{-/-}$ mice exhibited a reduced proportion of intrathymic DCs capturing OVA protein compared with WT mice (Fig. 8, *A* and *B*). Moreover, after the OVA_{647} injection, Sirpα$^+$ DCs of WT mice contained a substantial proportion of OVA^{high} cells, which represent the cells with a higher uptake of OVA protein, and this population was markedly reduced in $CCR2^{-/-}$ mice (Fig. 8, *C* and *D*). Moreover, among Sirpα$^+$ DCs, the CCR2-expressing population was a main cell type which captured OVA protein (Fig. 8*E*). CMFDA-labeled WT mouse-derived bone marrow cells appeared in thymus 2 days after the adoptive transfer to CCR2-deficient mice and a substantial proportion of these stained cells expressed CD11c and Sirpα simultaneously (Fig. 8*F*). Sirpα$^+$CD11c$^+$ DCs appeared in thymus similarly when CMFDA-labeled CCR2-deficient mouse-derived bone marrow cells were adoptively transferred (data not shown). When OVA_{647} was injected i.v. 2 days after the adoptive transfer, WT donor-derived Sirpα$^+$CD11c$^+$ DCs captured OVA protein more efficiently than CCR2-deficient DCs in the CCR2-deficient thymus (Fig. 8*G*). Thus, CCR2-mediated signals may at least partially regulate the function of Sirpα$^+$ DCs to uptake Ag from the bloodstream (supplemental Fig. S6).

Accumulation of autoreactive T cells against serum Ags in the periphery of $CCR2^{-/-}$ mice

We observed that $CCR2^{-/-}$ mice did not exhibit any signs suggestive of autoimmune disorders until 1 year after the birth (our unpublished data). Hence, we examined whether autoreactive T cells against certain self-Ags in the bloodstream accumulated in the periphery of $CCR2^{-/-}$ mice. We examined the accumulation of autoreactive T cells in the draining lymph nodes in WT mice that received CFSE-labeled WT or $CCR2^{-/-}$ mouse-derived splenocytes and were subsequently immunized with mouse serum emulsified in CFA. Immunization with total serum protein increased the cell division of $CCR2^{-/-}$ mouse-derived CD4$^+$ T cells inside draining lymph nodes (10.6%) to a greater extent than immunization with PBS (4.3%; Fig. 9*A*). Moreover, CD4$^+$ T cell division was significantly increased in the recipients of $CCR2^{-/-}$ mouse-derived splenocytes compared with the recipients of WT mouse-derived splenocytes (Fig. 9*B*). Thus, the lack of CCR2 can

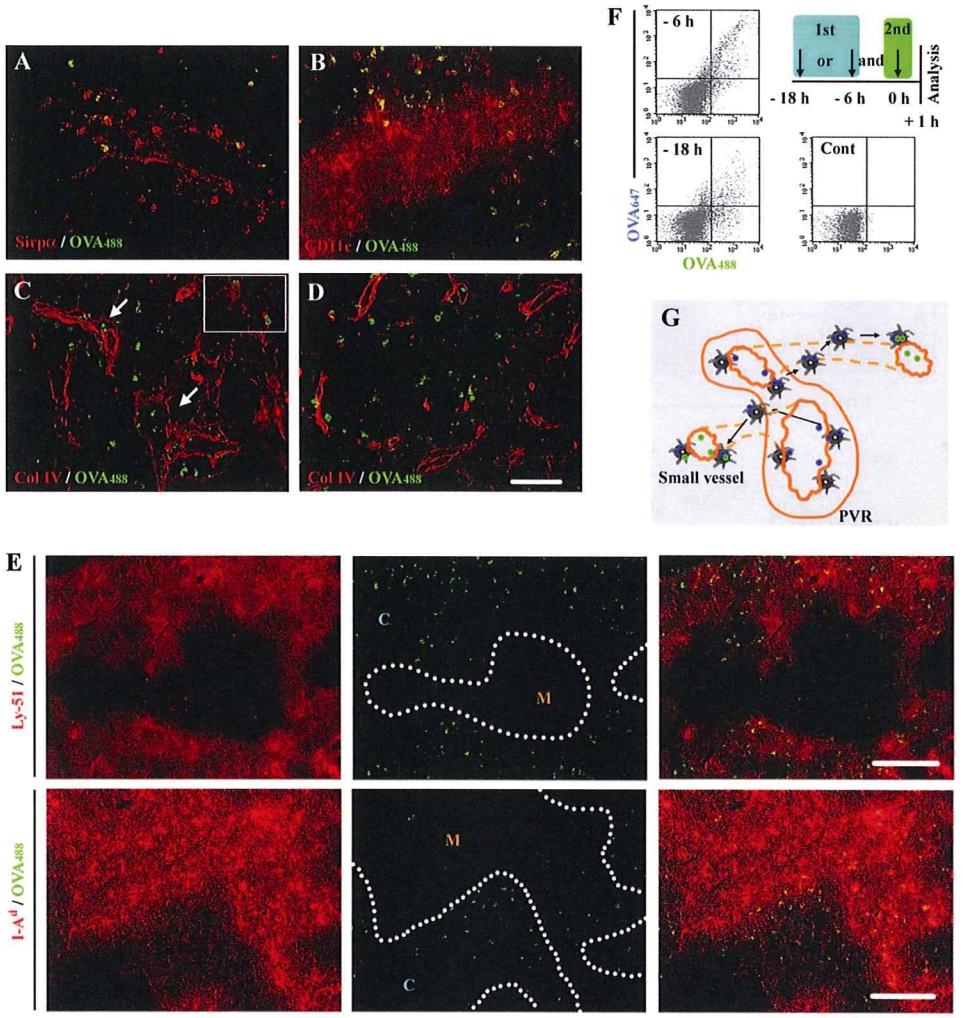

FIGURE 5. Localization of i.v. injected Ag in thymus. *A–C*, Thymic tissues were obtained 0.5 h after injection of OVA_{488} and were stained to obtain a double-color fluorescent image with the combination of OVA_{488} (green) and (*A*) Sirpα (red), (*B*) CD11c (red), or (*C*) Col IV (red). Arrows in *C* indicate the cells with captured OVA_{488} inside the PVRs. The image showing the cells capturing OVA_{488} in close proximity to small vessels is an *inset* in *C*. *D*, A double-color fluorescent image for OVA_{488} (green) and Col IV (red) at 6 h after OVA injection. Scale bars, 100 μm. *E*, A double-color fluorescent image with the combination of OVA_{488} (green) and Ly51 (red) or I-A^d (red) at 18 h after injection is shown in the *upper* and *lower panels*, respectively. The merged images are shown in the *right panels*. Dashed lines indicate the boundary between cortex (C) and medulla (M). Scale bars, 200 μm. *F*, OVA_{647} and OVA_{488} were i.v. injected consequently with an interval of either 6 or 18 h, illustrated in *upper right panel* in *F*. Uptake of OVA protein by $CD11c^{high}$ DC population isolated after double injection with an interval of either 6 or 18 h is shown in the *left upper* and *lower panels*, respectively. Autofluorescence for each parameter in the $CD11c^{high}$ DC population without injection is shown as a control. Representative results from three independent experiments are shown here. *G*, Presumed intrathymic trafficking modes of $Sirp\alpha^+$ DCs, combined with the Ag uptake. Blue and green particles indicate OVA_{647} and OVA_{488}, respectively.

result in enhanced accumulation of autoreactive T cells against serum self-Ags.

Discussion

Mouse thymus $CD11c^+$ cDCs can be classified into two populations, a major $CD8\alpha^+$ and a minor $CD8\alpha^-$ one (31). $CD8\alpha^-$ cDCs can pick up $CD8\alpha\beta$ heterodimer from thymocytes and retain them on the cell surface, thus precluding the use of $CD8\alpha$ as a reliable marker to distinguish these two populations. Wu and Shortman (8) observed that $CD8\alpha^-$ but not $CD8\alpha^+$ cDCs simultaneously express the Sirpα molecule and proposed the use of Sirpα as a marker of this minor cDC population. Concomitantly, it was proposed that the interaction between thymocytes and DCs in thymic cortex can also have profound effects on positive selection (32). Likewise, McCaughtry et al. (33) observed that clonal deletion of autoreactive thymocytes requires the stimuli from rare $CD11c^+$ cortical DCs. Given the unique localization of $Sirp\alpha^+$ DCs confined to the cortex, these observations suggest the potential involvement of $Sirp\alpha^+$ DCs in central tolerance, but their small number hinders the isolation for a detailed analysis of $Sirp\alpha^+$ DC function.

A partial but selective reduction in intrathymic $Sirp\alpha^+$ cDCs in $CCR2^{-/-}$ mice prompted us to investigate the thymic selection process in WT and $CCR2^{-/-}$ mice to elucidate the role of intrathymic $Sirp\alpha^+$ cDCs in the process. When DO11.10 TCR-transgenic mice were administered immunogenic $OVA_{323-339}$ peptide i.v., *CCR2* gene ablation partially attenuated the clonal negative deletion by apoptosis of the $DO11.10^+$ DP thymocyte population. Intraperitoneal injection of anti-CD3 Ab deleted thymocytes to similar extents in WT and $CCR2^{-/-}$ mice, excluding the possibility that CCR2 deficiency impaired the apoptotic response of thymocytes. Negative selection can be exerted by various types of APCs including $Sirp\alpha^-$ cDCs, B cells, macrophages, cortical thymic epithelial cells, and mTEC in addition to $Sirp\alpha^+$ cDCs. We

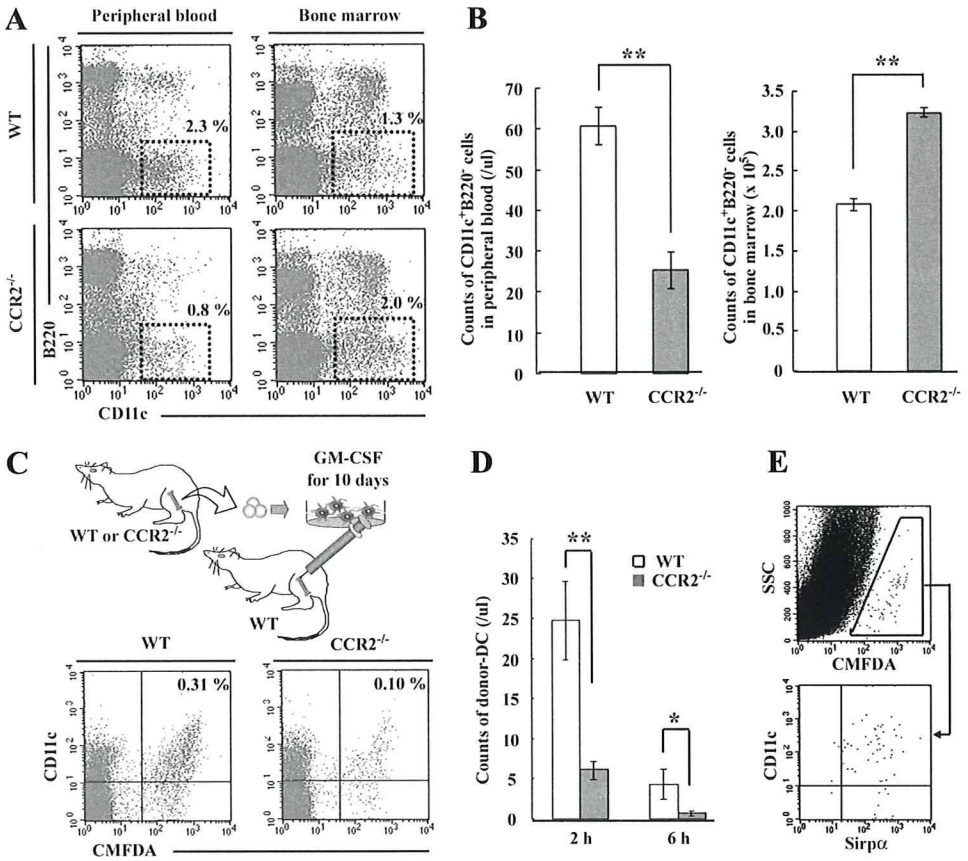

FIGURE 6. Mobilization of Sirpα+ DCs from bone marrow. *A* and *B*, PBMCs and bone marrow cells isolated from femur bone marrow were stained with anti-CD11c and anti-B220 mAbs. Proportion (*A*) and the numbers (*B*) of $CD11c^+B220^-$ cells gated with the dot squares were determined on peripheral blood and bone marrow in $CCR2^{-/-}$ and WT mice. Percentage of gated cells is shown in each panel of *A*. Mean ± SD were calculated from three independent experiments and are shown here. *C*, The image of experimental procedure of "trafficking of bone marrow-derived DCs" was illustrated and is shown in the *upper panel*. PBMCs were isolated from the recipients 2 h after injection and stained with anti-CD11c mAb. Egress of $CCR2^{-/-}$ bone marrow-derived DCs into peripheral blood was compared with WT DCs. Percentage of donor DCs in $CMFDA^+CD11c^+$ region is shown in each panel. *D*, The numbers of donor-derived DCs in peripheral blood were determined 2 and 6 h after injection. Mean ± SD calculated from five independent experiments are shown here. *, $p < 0.05$ and **, $p < 0.01$. *E*, One × 10^7 WT bone marrow cell-derived DCs were injected into both the right and left tibial cavity. Six hours after injection, expression of Sirpα and CD11c on intrathymic migrated $CMFDA^+$ donor cells was analyzed by FCM. Representative results from four independent experiments are shown here.

failed to detect any apparent differences in other APC populations than Sirpα+ cDCs between WT and $CCR2^{-/-}$ mice. Thus, it is unlikely that reduced negative selection in $CCR2^{-/-}$ mice can be ascribed to the changes in these cell populations. Furthermore, accumulating evidence implicates intrathymic $CD4^+CD25^+$ regulatory T cells as an essential cell component in central tolerance.

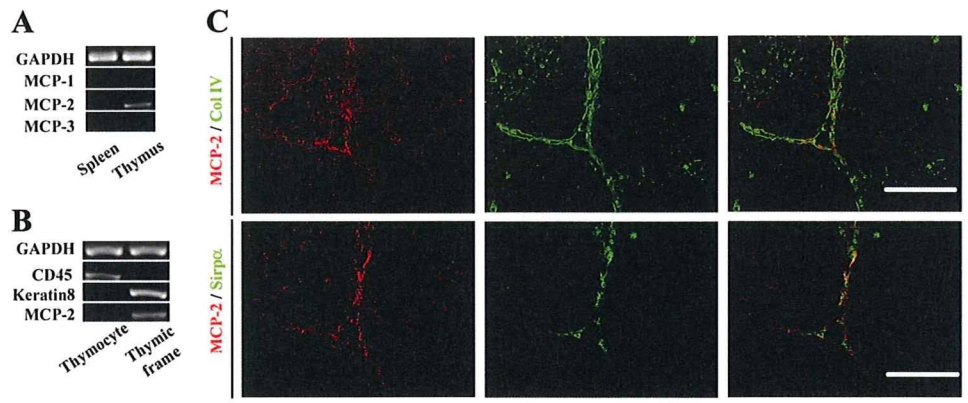

FIGURE 7. Expression of CCR2 ligands in thymus under physiological condition. *A*, Total RNAs were extracted from thymus and spleen of WT mice. Expression of CCR2 ligands, MCP-1, MCP-2, and MCP-3, was determined by RT-PCR. GAPDH served as an internal positive control. *B*, Thymic tissues were mechanically disrupted and fractionated into thymocyte and thymic stromal components. MCP-2 transcripts were determined on these two fractions by RT-PCR. CD45 and keratin 8 served as positive control for the thymocyte and thymic stromal fraction, respectively. *C*, Double-color fluorescent immunostaining for MCP-2 (red) and Col IV (green) or MCP-2 (red) and Sirpα (green) in the thymic tissue sections are shown in the *upper* and *lower panels*, respectively. The merged images are shown in the *right panels*. Representative results from three independent animals are shown here. Scale bars, 100 μm.

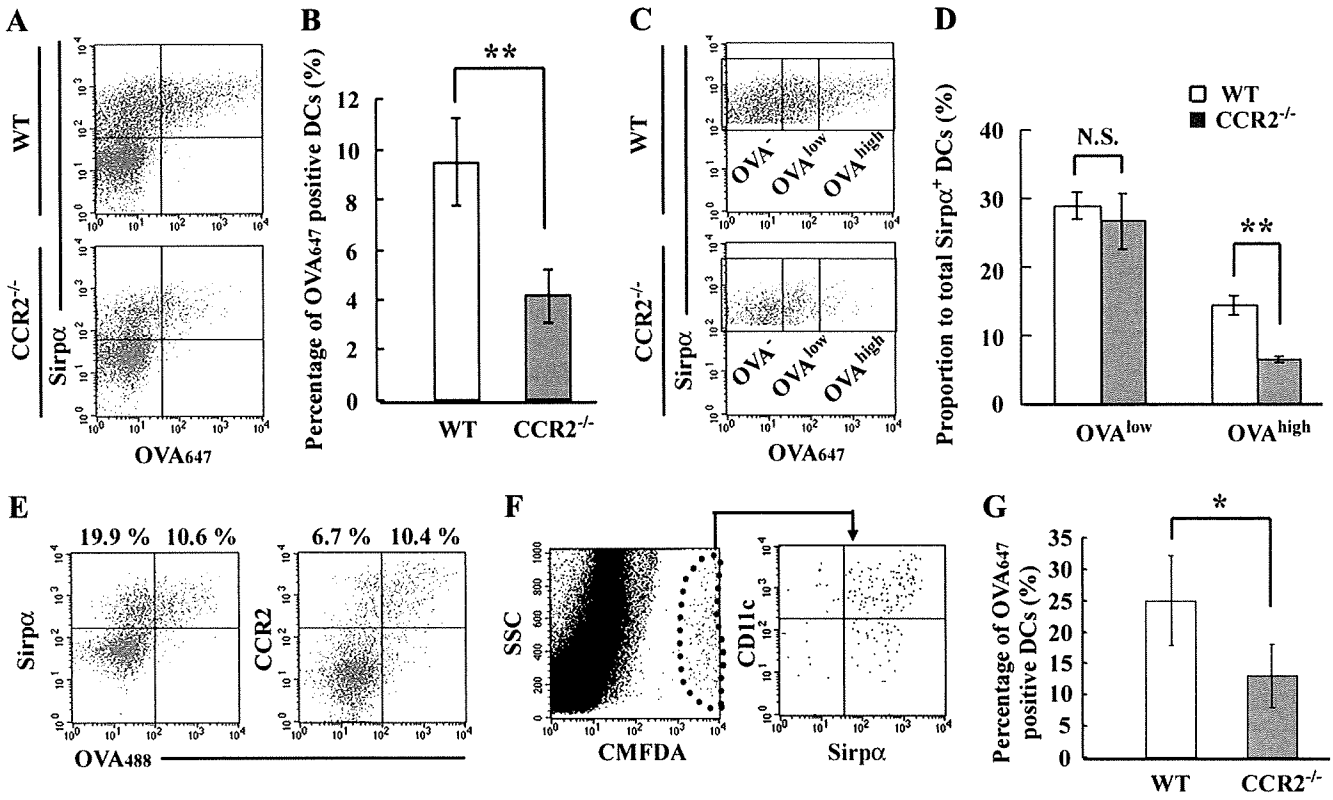

FIGURE 8. Effects of CCR2 deficiency on Ag uptake by thymic Sirpα$^+$ DCs. *A*, The uptake of OVA_{647} in the CCR2$^{-/-}$ CD11c^{high} DC population at 4 h after i.v. injection was compared with WT-derived cells. *B*, Percentage of DCs capturing OVA_{647} in the CD11c^{high} DC population. Mean ± SD were calculated from five independent experiments and are shown here. **, $p < 0.01$ *C*, Sirpα$^+$ DCs derived from WT and CCR2$^{-/-}$ thymus were separated into three groups according to the efficiency of OVA_{647} uptake, OVA$^-$; DCs without capturing OVA_{647}, OVA^{low}; DCs capturing OVA_{647} with a low efficiency, and OVA^{high}; and DCs capturing OVA_{647} with a high efficiency. *D*, Percentage of OVA^{low} and OVA^{high} in WT and the CCR2$^{-/-}$ Sirpα$^+$ DC population. Mean ± SD were calculated from five independent experiments and are shown here. **, $p < 0.01$; N.S., no significant difference. *E*, OVA_{488} was i.v. injected into WT mice. One hour after injection, low-density cells were stained with anti-CD11c and anti-Sirpα or anti-CCR2 mAbs. The uptake of OVA_{488} and expression of Sirpα or CCR2 in the CD11c^{high} DC population are shown. Percentage of Sirpα$^+$OVA$_{488}^+$ and OVA$_{488}^-$, or CCR2$^+$OVA$_{488}^+$ and OVA$_{488}^-$ regions are shown in the *left* or *right panel*. Representative results from three independent experiments are shown here. *F*, Migration of Sirpα$^+$ DCs into the thymus at 2 days after i.v. injection of CMFDA-labeled WT bone marrow cells into CCR2$^{-/-}$ mice. Expression of CD11c and Sirpα on CMFDA$^+$ donor-derived cells is shown in the *right panel*. Representative results from three independent experiments are shown here. *G*, OVA_{647} was i.v. injected into CCR2$^{-/-}$ mice at 2 days after injection of bone marrow cells. Percentage of WT and CCR2$^{-/-}$ donor-derived DCs capturing OVA_{647} in the CMFDA$^+$CD11c^{high} region are shown. Mean ± SD were calculated from four independent experiments and are shown here. *, $p < 0.05$.

Indeed, Proietto et al. (14) recently reported the capability of Sirpα$^+$ cDCs to induce the differentiation of regulatory T cells in vitro. However, OVA peptide injection induced the differentiation of regulatory T cells to similar extents in both DO11.10 and DO11.10/CCR2$^{-/-}$ thymus. Thus, it is probable that CCR2 deficiency reduced modestly intrathymic Sirpα$^+$ DCs without affecting regulatory cell induction and partially attenuated negative selection in vivo.

It remains elusive on the trafficking modes of Sirpα$^+$ DCs. In CCR2$^{-/-}$ mice, Sirpα$^+$ DCs were decreased moderately in peripheral blood and thymus, but were increased in bone marrow. Considering that CCR2 signaling can regulate the mobilization of monocytes from bone marrow to peripheral blood (34, 35), these observations raised the possibility of a defect in the trafficking of Sirpα$^+$ DCs from bone marrow in CCR2$^{-/-}$ mice. Indeed, WT mouse-derived Sirpα$^+$ DCs, injected into bone marrow, appeared first in peripheral blood and then the thymus. On the contrary, CCR2$^{-/-}$ mouse-derived Sirpα$^+$ DCs exhibited impairment in the egress from bone marrow to peripheral blood. These observations suggest that bone marrow-derived Sirpα$^+$ DCs migrated to peripheral blood in response to CCR2-mediated signals and subsequently traffic to the thymus.

In the thymus, Sirpα$^+$ DCs were characteristically localized in close proximity to small blood vessels and inside the PVRs, sites which are compartmentalized by a vascular basement membrane and a border membrane separating them from the thymic parenchyma (36). It is of note that Sirpα$^+$ cells in the PVRs were markedly decreased in CCR2$^{-/-}$ mice to a greater extent than the decrease in total Sirpα$^+$ cell number. Thus, intrathymic CCR2 signaling can regulate their unique localization. This notion was supported by the observation that MCP-2, a potential ligand for CCR2, was constitutively detected in the PVRs, where Sirpα$^+$ DCs were present.

PVRs can provide a pathway for hematopoietic progenitor cells and mature T cells to traverse from the bloodstream to the thymic parenchyma (36) and are presumed to constitute the blood-thymus barrier, which can protect the thymic parenchyma from bloodstream-derived macromolecules (28). Thus, the unique localization of Sirpα$^+$ cDCs in the thymus suggested their potential interactions with bloodstream-derived Ag. This assumption was strengthened by our present observation that intrathymic Sirpα$^+$ cDCs rapidly and specifically captured OVA protein and serum IgG following i.v. injection. Moreover, injected Ags were initially detected inside PVRs or in nearby small vessels and were subsequently in the cortical parenchyme, and the injected Ag-derived

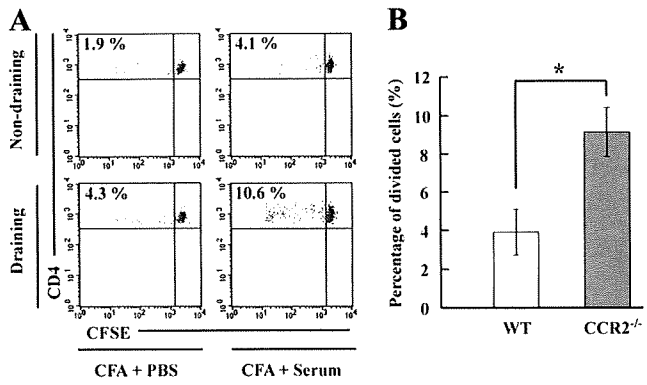

FIGURE 9. Accumulation of autoreactive T cells against serum Ags in the spleen. Spleen mononuclear cells were isolated from WT or $CCR2^{-/-}$ mice and i.v. injected into WT mice after labeling with CFSE. *A*, Recipients of $CCR2^{-/-}$ mouse-derived splenocytes were immunized with total mouse serum or PBS emulsified in CFA at 1 day after injection. Four days after, draining and nondraining lymph nodes were harvested and division of $CFSE^+$ donor-derived $CD4^+$ T cells was analyzed by FCM. Representative results from three independent experiments are shown here. *B*, Percentage of divided $CD4^+$ T cells was determined in the draining lymph nodes of the recipients of either WT-derived or $CCR2^{-/-}$ donor-derived splenocytes when the recipients were immunized with mouse serum emulsified in CFA. Mean ± SD were calculated from three independent experiments and are shown here. *, $p < 0.01$.

signals were consistently colocalized with CD11c and Sirpα. Thus, after $CD11c^+Sirp\alpha^+$ cDCs, located around the PVRs, capture the Ags, they presumably move to cortical parenchyme to educate T cells. Indeed, $CCR2^{-/-}$ thymus-derived $Sirp\alpha^+$ DCs exhibited a reduced capacity to uptake OVA. The lack of CCR2 can hinder the proper intrathymic localization of $Sirp\alpha^+$ DCs and their distinctive function, Ag uptake from bloodstream, thereby reducing Ag presentation in the cortical parenchyma and subsequent negative selection against a blood-borne Ag. This hypothesis is supported by our observation in that $CD4^+$ T cells reactive to certain serum self-Ags accumulated in the periphery of the recipients of $CCR2^{-/-}$ mouse-derived splenocytes to a greater extent than the recipients of WT mouse-derived splenocytes.

DCs can uptake free soluble Ags, in three distinct manners, by clathrin-mediated endocytosis, nonclathrin/caveolae endocytosis, and macropinocytosis (25). Thymic $Sirp\alpha^+$ cDCs could endocytose OVA Ags more efficiently than thymic $Sirp\alpha^-$ cDCs when they were cultured in vitro with OVA Ags. Furthermore, NH_4Cl, an inhibitor of clathrin-mediated endocytosis (26), markedly inhibited OVA endocytosis by $Sirp\alpha^+$ cDCs, but not by $Sirp\alpha^-$ cDCs. On the contrary, OVA protein endocytosis by $Sirp\alpha^-$ DCs was partially inhibited by mannan, whereas mannan had few effects on OVA protein endocytosis by $Sirp\alpha^+$ DCs. These observations suggest that thymic $Sirp\alpha^+$ cDCs characteristically can efficiently endocytose Ags in a manner distinct from thymic $Sirp\alpha^-$ cDCs.

Balazs et al. (29) reported that bloodstream DCs could efficiently capture and transport particulate bacteria into the spleen when particulate bacteria were i.v. injected. We also observed that $CD11c^+$ DCs rapidly disappeared from peripheral blood after uptake of i.v. injected OVA protein. Given the capacity of $CD11c^+$ DCs to move rapidly from blood to thymus, blood $CD11c^+$ DCs may migrate into thymus after capturing the i.v. injected Ag. However, Ag-capturing DCs appeared very rapidly in the thymus, reaching maximal levels before disappearance of Ag-capturing circulating DCs from the peripheral blood. Furthermore, when OVA protein was injected i.v. into mice that contained bloodstream DCs labeled with fluorescent-conjugated latex beads, latex-labeled DCs did not appear in the thymus (our unpublished data). Thus, it is remotely possible that bloodstream DCs captured OVA protein and subsequently migrated into thymus.

In this study, we identified the unique intrathymic localization and functions of thymic $Sirp\alpha^+$ DCs that are involved in negative selection, particularly against blood-borne Ags. Serum protein can also induce negative selection in thymus (27, 37) but the molecular and cellular mechanisms remain to be elucidated. Because $Sirp\alpha^+$ cDCs can uptake serum protein such as IgG, these cells may induce central tolerance to blood-borne-derived Ags, in addition to Ags presented by the well-characterized intrathymic AIRE-mediated pathway.

We have shown that CCR2-mediated signals can regulate various biological aspects of $Sirp\alpha^+$ DCs such as their appropriate intrathymic localization and Ag uptake capacity. It is widely held that CCR2 might be a potential therapeutic target for several autoimmune disorders. However, because CCR2-mediated signals may contribute to thymic negative selection against blood-borne Ags, CCR2 blockade may aggravate autoimmune disorders similar to the observation on the murine collagen-induced arthritis model (38). Moreover, Lauritzsen et al (39) reported that proteins secreted from tumor cells into peripheral blood were transported into the thymus to eventually cause clonal deletion of tumor Ag-specific T cell repertoires. Given the potential capacity of intrathymic $Sirp\alpha^+$ DCs to capture blood-borne Ags, they may have a role in the development of tumor tolerance. Because human thymus contains DCs with similar phenotypes and intrathymic localization as $Sirp\alpha^+$ cDCs (40), a more detailed elucidation of the functions of $Sirp\alpha^+$ cDCs may provide us with useful insights to develop a better therapeutic strategy for cancer and stem cell transplantation as well as autoimmune disorders.

Acknowledgments

We express our gratitude to Drs. Joost J. Oppenheim (National Cancer Institute-Frederick, Frederick, MD) and Nobuyuki Onai (Akita University, Akita, Japan), and Yi Zhang (University of Michigan, Ann Arbor, MI) for critical review of this manuscript. We thank Drs. William Kuziel, Kouji Matsushima, and Philip Murphy for providing us with CCR2-, CCR5-, and CCR1- and CX3CR1-deficient mice, respectively.

Disclosures

The authors have no financial conflict of interest.

References

1. von Boehmer, H., I. Aifantis, F. Gounari, O. Azogui, L. Haughn, I. Apostolou, E. Jaeckel, F. Grassi, and L. Klein. 2003. Thymic selection revisited: how essential is it? *Immunol. Rev.* 191: 62–78.
2. Anderson, M. S., E. S. Venanzi, Z. Chen, S. P. Berzins, C. Benoist, and D. Mathis. 2005. The cellular mechanism of Aire control of T cell tolerance. *Immunity* 23: 227–239.
3. Anderson, M. S., E. S. Venanzi, L. Klein, Z. Chen, S. P. Berzins, S. J. Turley, H. von Boehmer, R. Bronson, A. Dierich, C. Benoist, and D. Mathis. 2002. Projection of an immunological self shadow within the thymus by the aire protein. *Science* 298: 1395–1401.
4. Liston, A., S. Lesage, J. Wilson, L. Peltonen, and C. C. Goodnow. 2003. Aire regulates negative selection of organ-specific T cells. *Nat. Immunol.* 4: 350–354.
5. Anderson, G., K. M. Partington, and E. J. Jenkinson. 1998. Differential effects of peptide diversity and stromal cell type in positive and negative selection in the thymus. *J. Immunol.* 161: 6599–6603.
6. Marrack, P., D. Lo, R. Brinster, R. Palmiter, L. Burkly, R. H. Flavell, and J. Kappler. 1988. The effect of thymus environment on T cell development and tolerance. *Cell* 53: 627–634.
7. Matzinger, P., and S. Guerder. 1989. Does T-cell tolerance require a dedicated antigen-presenting cell? *Nature* 338: 74–76.
8. Wu, L., and K. Shortman. 2005. Heterogeneity of thymic dendritic cells. *Semin. Immunol.* 17: 304–312.
9. Liu, Y. J. 2006. A unified theory of central tolerance in the thymus. *Trends Immunol.* 27: 215–221.
10. Bendriss-Vermare, N., C. Barthelemy, I. Durand, C. Bruand, C. Dezutter-Dambuyant, N. Moulian, S. Berrih-Aknin, C. Caux, G. Trinchieri, and F. Briere. 2001. Human

thymus contains IFN-α-producing CD11c$^-$, myeloid CD11c$^+$, and mature interdigitating dendritic cells. *J. Clin. Invest.* 107: 835–844.
11. Sprent, J., and S. R. Webb. 1995. Intrathymic and extrathymic clonal deletion of T cells. *Curr. Opin. Immunol.* 7: 196–205.
12. Heino, M., P. Peterson, N. Sillanpaa, S. Guerin, L. Wu, G. Anderson, H. S. Scott, S. E. Antonarakis, J. Kudoh, N. Shimizu, et al. 2000. RNA and protein expression of the murine *autoimmune regulator gene (Aire)* in normal, RelB-deficient and in NOD mouse. *Eur. J. Immunol.* 30: 1884–1893.
13. Kyewski, B., and J. Derbinski. 2004. Self-representation in the thymus: an extended view. *Nat. Rev. Immunol.* 4: 688–698.
14. Proietto, A. I., S. van Dommelen, P. Zhou, A. Rizzitelli, A. D'Amico, R. J. Steptoe, S. H. Naik, M. H. Lahoud, Y. Liu, P. Zheng, et al. 2008. Dendritic cells in the thymus contribute to T-regulatory cell induction. *Proc. Natl. Acad. Sci. USA* 105: 19869–19874.
15. Heinzel, K., C. Benz, and C. C. Bleul. 2007. A silent chemokine receptor regulates steady-state leukocyte homing in vivo. *Proc. Natl. Acad. Sci. USA* 104: 8421–8426.
16. Kim, C. H. 2005. The greater chemotactic network for lymphocyte trafficking: chemokines and beyond. *Curr. Opin. Hematol.* 12: 298–304.
17. Schutyser, E., A. Richmond, and J. Van Damme. 2005. Involvement of CC chemokine ligand 18 (CCL18) in normal and pathological processes. *J. Leukocyte Biol.* 78: 14–26.
18. Vecchi, A., L. Massimiliano, S. Ramponi, W. Luini, S. Bernasconi, R. Bonecchi, P. Allavena, M. Parmentier, A. Mantovani, and S. Sozzani. 1999. Differential responsiveness to constitutive vs. inducible chemokines of immature and mature mouse dendritic cells. *J. Leukocyte Biol.* 66: 489–494.
19. Niess, J. H., S. Brand, X. Gu, L. Landsman, S. Jung, B. A. McCormick, J. M. Vyas, M. Boes, H. L. Ploegh, J. G. Fox, et al. 2005. CX3CR1-mediated dendritic cell access to the intestinal lumen and bacterial clearance. *Science* 307: 254–258.
20. Gao, J. L., T. A. Wynn, Y. Chang, E. J. Lee, H. E. Broxmeyer, S. Cooper, H. L. Tiffany, H. Westphal, J. Kwon-Chung, and P. M. Murphy. 1997. Impaired host defense, hematopoiesis, granulomatous inflammation and type 1-type 2 cytokine balance in mice lacking CC chemokine receptor 1. *J. Exp. Med.* 185: 1959–1968.
21. Combadiere, C., S. Potteaux, J. L. Gao, B. Esposito, S. Casanova, E. J. Lee, P. Debre, A. Tedgui, P. M. Murphy, and Z. Mallat. 2003. Decreased atherosclerotic lesion formation in CX3CR1/apolipoprotein E double knockout mice. *Circulation* 107: 1009–1016.
22. Murai, M., H. Yoneyama, T. Ezaki, M. Suematsu, Y. Terashima, A. Harada, H. Hamada, H. Asakura, H. Ishikawa, and K. Matsushima. 2003. Peyer's patch is the essential site in initiating murine acute and lethal graft-versus-host reaction. *Nat. Immunol.* 4: 154–160.
23. Kuziel, W. A., S. J. Morgan, T. C. Dawson, S. Griffin, O. Smithies, K. Ley, and N. Maeda. 1997. Severe reduction in leukocyte adhesion and monocyte extravasation in mice deficient in CC chemokine receptor 2. *Proc. Natl. Acad. Sci. USA* 94: 12053–12058.
24. Brewer, J. A., O. Kanagawa, B. P. Sleckman, and L. J. Muglia. 2002. Thymocyte apoptosis induced by T cell activation is mediated by glucocorticoids in vivo. *J. Immunol.* 169: 1837–1843.
25. Mayor, S., and R. E. Pagano. 2007. Pathways of clathrin-independent endocytosis. *Nat. Rev. Mol. Cell Biol.* 8: 603–612.
26. Sandvig, K., S. Olsnes, O. W. Petersen, and B. van Deurs. 1987. Acidification of the cytosol inhibits endocytosis from coated pits. *J. Cell Biol.* 105: 679–689.
27. Zal, T., A. Volkmann, and B. Stockinger. 1994. Mechanisms of tolerance induction in major histocompatibility complex class II-restricted T cells specific for a blood-borne self-antigen. *J. Exp. Med.* 180: 2089–2099.
28. Bubanovic, I. V. 2003. Failure of blood-thymus barrier as a mechanism of tumor and trophoblast escape. *Med. Hypotheses* 60: 315–320.
29. Balazs, M., F. Martin, T. Zhou, and J. Kearney. 2002. Blood dendritic cells interact with splenic marginal zone B cells to initiate T-independent immune responses. *Immunity* 17: 341–352.
30. Murphy, P. M., M. Baggiolini, I. F. Charo, C. A. Hebert, R. Horuk, K. Matsushima, L. H. Miller, J. J. Oppenheim, and C. A. Power. 2000. International union of pharmacology: XXII. Nomenclature for chemokine receptors. *Pharmacol. Rev.* 52: 145–176.
31. Vremec, D., J. Pooley, H. Hochrein, L. Wu, and K. Shortman. 2000. CD4 and CD8 expression by dendritic cell subtypes in mouse thymus and spleen. *J. Immunol.* 164: 2978–2986.
32. Ladi, E., T. A. Schwickert, T. Chtanova, Y. Chen, P. Herzmark, X. Yin, H. Aaron, S. W. Chan, M. Lipp, B. Roysam, and E. A. Robey. 2008. Thymocyte-dendritic cell interactions near sources of CCR7 ligands in the thymic cortex. *J. Immunol.* 181: 7014–7023.
33. McCaughtry, T. M., T. A. Baldwin, M. S. Wilken, and K. A. Hogquist. 2008. Clonal deletion of thymocytes can occur in the cortex with no involvement of the medulla. *J. Exp. Med.* 205: 2575–2584.
34. Sawanobori, Y., S. Ueha, M. Kurachi, T. Shimaoka, J. E. Talmadge, J. Abe, Y. Shono, M. Kitabatake, K. Kakimi, N. Mukaida, and K. Matsushima. 2008. Chemokine-mediated rapid turnover of myeloid-derived suppressor cells in tumor-bearing mice. *Blood* 111: 5457–5466.
35. Tsou, C. L., W. Peters, Y. Si, S. Slaymaker, A. M. Aslanian, S. P. Weisberg, M. Mack, and I. F. Charo. 2007. Critical roles for CCR2 and MCP-3 in monocyte mobilization from bone marrow and recruitment to inflammatory sites. *J. Clin. Invest.* 117: 902–909.
36. Mori, K., M. Itoi, N. Tsukamoto, H. Kubo, and T. Amagai. 2007. The perivascular space as a path of hematopoietic progenitor cells and mature T cells between the blood circulation and the thymic parenchyma. *Int. Immunol.* 19: 745–753.
37. Haribhai, D., D. Engle, M. Meyer, D. Donermeyer, J. M. White, and C. B. Williams. 2003. A threshold for central T cell tolerance to an inducible serum protein. *J. Immunol.* 170: 3007–3014.
38. Quinones, M. P., S. K. Ahuja, F. Jimenez, J. Schaefer, E. Garavito, A. Rao, G. Chenaux, R. L. Reddick, W. A. Kuziel, and S. S. Ahuja. 2004. Experimental arthritis in CC chemokine receptor 2-null mice closely mimics severe human rheumatoid arthritis. *J. Clin. Invest.* 113: 856–866.
39. Lauritzsen, G. F., P. O. Hofgaard, K. Schenck, and B. Bogen. 1998. Clonal deletion of thymocytes as a tumor escape mechanism. *Int. J. Cancer* 78: 216–222.
40. Paessens, L. C., D. M. Fluitsma, and Y. van Kooyk. 2008. Haematopoietic antigen-presenting cells in the human thymic cortex: evidence for a role in selection and removal of apoptotic thymocytes. *J. Pathol.* 214: 96–103.

Case Report

Digestion

Digestion 2009;79:36–39
DOI: 10.1159/000203639

Published online: February 25, 2009

Pegylated Interferon plus Ribavirin Combination Therapy for Chronic Hepatitis C with High Viral Load of Serum Hepatitis C Virus RNA, Genotype 1b, Discontinued on Attaining Sustained Virological Response at Week 16 after Onset of Acute Pancreatitis

Soo Ryang Kim[c] Susumu Imoto[c] Keiji Mita[c] Miyuki Taniguchi[c] Noriko Sasase[c] Akira Muramatsu[a] Masatoshi Kudo[b] Satoshi Kitai[b] Ahmed El-Shamy[d] Hak Hotta[d] Yoshitake Hayashi[e]

[a]Division of Liver Diseases, Meimai Central Hospital, Akashi, [b]Department of Gastroenterology and Hepatology, Kinki University School of Medicine, Osaka-Sayama, [c]Department of Gastroenterology, Kobe Asahi Hospital, [d]Division of Microbiology, and [e]Division of Molecular Medicine and Medical Genetics, International Center for Medical Research and Treatment, Kobe University Graduate School of Medicine, Kobe, Japan

Key Words
Acute pancreatitis · Chronic hepatitis C · Early viral dynamics, genotype 1b · Sustained virological response

Abstract
Recent clinical trials have shown that pegylated interferon-α (PEG-IFN-α) in combination with ribavirin (RBV) improves the rate of sustained virological response (SVR), with over 50% of patients demonstrating a positive response to treatment. However, no SVR has been reported when PEG-IFN/RBV combination therapy is discontinued by week 16, especially in cases of chronic hepatitis with a high viral load of serum hepatitis C virus (HCV) RNA, genotype 1b. Here, we describe SVR in a 67-year-old woman whose PEG-IFN/RBV combination therapy for chronic hepatitis C with a high viral load of serum HCV RNA, genotype 1b, was discontinued after 16 weeks because of the onset of PEG-IFN plus RBV-induced acute pancreatitis. Among viral factors, substitution of amino acid 70 (Arg) and 91 (Leu) in the core region and HCV RNA negativity were observed after 8 weeks. Host factors including low body weight, no alcohol consumption, no coinfection with hepatitis B virus, slight fibrosis, and viral factors including early viral clearance, double wild type in the core region, may have contributed to the SVR irrespective of the discontinuation of the combination therapy at week 16. Moreover, PEG-IFN plus RBV-induced acute pancreatitis might have been related to the SVR.

Introduction

In Japan, about 70% of chronic hepatitis C (CHC) patients are infected with genotype 1b, the rest with genotype 2a/2b [1]. Of the former, almost 70% demonstrate a high viral load, a crucial risk factor for poor response to antiviral treatment, as are the host-related factors of age, obesity, female gender and hepatic fibrosis [2, 3].

The rate of sustained virological response (SVR) can be increased to approximately 40% through 48 weeks of interferon (IFN)-α2b and ribavirin (RBV) combination

KARGER
Fax +41 61 306 12 34
E-Mail karger@karger.ch
www.karger.com

0012–2823/09/0791–0036$26.00/0

Accessible online at:
www.karger.com/dig

Soo Ryang Kim, MD
Department of Gastroenterology, Kobe Asahi Hospital
3-5-25 Bououji-cho, Nagata-ku, Kobe 653-0801 (Japan)
Tel. +81 78 612 5151, Fax +81 78 612 5152
E-Mail asahi-hp@arion.ocn.ne.jp

therapy for chronic hepatitis with a high viral load of serum hepatitis C virus (HCV) RNA, genotype 1b [4–6]. Pegylated (PEG)-IFN-α plus RBV therapy improves the SVR rate even further, with over 50% of patients responding positively to treatment [6]. Attaining the SVR irrespective of discontinuing combination therapy by week 16 has not been reported, even in cases of rapid virological response by CHC with a high viral load of serum HCV RNA, genotype 1b [7, 8].

Acute pancreatitis is an uncommon side effect of IFN-α and RBV combination therapy, and only few cases have been reported in the English literature [9]. It has also been diagnosed in 7 of 1,706 HCV-infected patients (0.4%; 95% CI 0.2–0.8) thus treated [10]. We present the case of a 67-year-old woman with chronic hepatitis and a high viral load of serum HCV RNA, genotype 1b, attaining SVR and discontinuing the therapy after 16 weeks because of the onset of acute pancreatitis after 14 weeks of therapy.

Case Report

A 67-year-old woman with CHC was admitted to Kobe Asahi Hospital in September 2007 for treatment of abdominal pain. In June 2007, she had been started on a weekly subcutaneous injection of 60 μg of PEG-IFN-α2b and a daily oral dose of 600 mg RBV at 44 kg of body weight. Reverse transcription polymerase chain reaction (PCR) revealed 2,300 and 1,900 kIU/ml of HCV RNA in May 2007 and June 2007, respectively. Hepatitis B surface antigen and hepatitis B virus DNA were negative, HCV core antigen by a new immunoradiometric (IRM) assay was 5,550 fmol/l, and the genotype was 1b. Laboratory tests revealed the following: total protein 6.2 g/dl (normal, 6.5–8.3), albumin 3.8 g/dl (3.8–5.3), aspartate aminotransferase 40 IU/l (0–38), alanine aminotransferase 29 IU/l (0–19), platelets 13.9 × 10^4/μl (14–34); liver biopsy revealed stage 1 fibrosis. Immunological examinations revealed the following: immunoglobulin G (IgG) 1,460 mg/dl (normal, 870–1,700), IgM 168 mg/dl (33–190), IgA 76 mg/dl (110–410), B cells 4% (4–13), T cells 90% (66–89), CD4/CD8 ratio 1.17% (0.40–2.30) and natural killer cell activity 50% (18–40).

Viral factors considered to be related to SVR [11–14] were as follows: 4 IFN/RBV resistance-determining region mutants (SVR is related to more than 6), 0 IFN sensitivity-determining region mutants (SVR is related to more than 4), and the core protein was the double wild type (Arg 70/Leu 91; SVR is related to the double wild type). Regarding early viral dynamics, HCV core antigen was 1,670 fmol/l at 24 h, 118 fmol/l at 1 week and <20 fmol/l at 2 weeks after treatment; it was <20 fmol/l, irrespective of HCV RNA positivity, 4 weeks after treatment. After 8 weeks, HCV RNA by the Amplicore PCR method was undetectable (<50 copies/ml) and liver functions were normal.

The patient tolerated therapy well until week 14, when she was admitted to our hospital with severe epigastric pain radiating to her back, nausea and vomiting. Laboratory tests revealed the following: amylase 178 IU/l (normal, 38–136), lipase 521 IU/l (23–300), aspartate aminotransferase 29 IU/l, alanine aminotransferase 10 IU/l, alkaline phosphokinase 226 IU/l (110–354), total bilirubin 0.5 mg/dl (0.2–1.2), white blood cell count 50 × 10^2/μl (40–90), calcium 9.4 mg/dl (8.7–10.1), total cholesterol 140 mg/dl (150–219), triglycerides 153 mg/dl (50–149), IgG4 20.1 mg/dl (48–105); all values, except for triglycerides and IgG4, were within normal limits. Tumor necrosis factor-α (TNF-α) and IL-6 were 8.8 pg/ml (<5.0) and 3.4 pg/ml (<4.0), respectively. The patient had no history of pancreatitis, denied alcohol use and was not taking any medications. Imaging studies such as ultrasound, computed tomography and magnetic resonance imaging revealed no swelling of the pancreas or dilation of the pancreatic duct. The gallbladder appeared normal and no biliary microgallstones were noted.

PEG-IFN-α2b and RBV were discontinued 16 weeks after the start of therapy, and the patient was treated with ulinastatin 150,000 units/day for 4 weeks and camostat mesilate 600 mg/day (oral dose) for 2 weeks under the diagnosis of acute pancreatitis. The pancreatitis was resolved and the patient was discharged in December 2007.

PEG-IFN-α2b and RBV therapy was discontinued and pancreatitis did not recur during 12 months of follow-up. Since January 2008, HCV has been undetectable (<15 copies/ml) by the TaqMan PCR method, and liver functions continued normal. The patient was evaluated as having attained SVR because HCV RNA disappeared 52 weeks after the discontinuation of therapy (fig. 1).

Discussion

Acute pancreatitis is a rare complication of PEG-IFN/RBV therapy. In our case, drug-induced acute pancreatitis was diagnosed on the basis of the presence of epigastric pain, elevated amylase and lipase levels, and the absence of other identifiable causes of pancreatitis. The patient showed no evidence of gallstones, alcohol consumption, or other potential causes of pancreatitis, such as autoimmune pancreatitis. These findings met the criteria for probable drug-induced pancreatitis [15, 16]. The onset of pancreatitis during PEG-IFN-α2b and RBV therapy and resolution of the symptoms after the discontinuation of treatment confirmed the diagnosis. Moreover, the absence of recurrent pancreatitis after the discontinuation of therapy also suggested that the medications were the most likely cause of acute pancreatitis.

IFN and RBV combination therapy is a potential cause of drug-induced pancreatitis in patients with chronic HCV. There are several potential mechanisms whereby IFN-α can cause pancreatitis. Treatment with IFN-α can result in severe hypertriglyceridemia [17–19], a well-described cause of acute pancreatitis [20]. However, in our case, severe hypertriglyceridemia was not observed. Alternatively, IFN-α may cause acute pancreatitis by stimu-

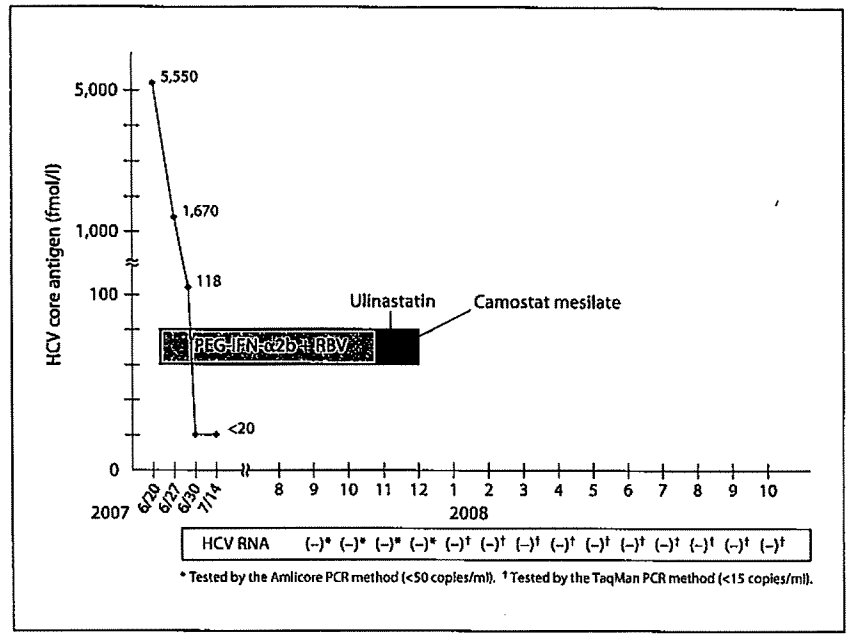

Fig. 1. Clinical course.

lating the immune system, leading to autoimmune destruction of the pancreas. In fact, IFN-α is known to precipitate or exacerbate other autoimmune disorders, such as thyroid disease, diabetes and others [21]. Based on the published literature, IFN-α is more likely to cause acute pancreatitis than RBV, although RBV is known to have immunomodulatory effects [22]; also, RBV, alone or synergistically with IFN-α, may stimulate the immune system to cause pancreatitis through an autoimmune mechanism. TNF-α is reported to induce acute pancreatitis [23]. In our case, high TNF-α may be markers of immune system stimulation due to PEG-IFN plus RBV or due to acute pancreatitis itself [24].

Predictors of the outcome of IFN-based therapy can be classified into pretreatment and on-treatment factors. The former comprise host factors such as age, sex, obesity, alcohol consumption, fibrosis, immune responses, as well as coinfection with other viruses, and the latter comprise viral factors that include mainly viral genotypes and viral load. In our case, viral genotype (genotype 1b) and high viral load (2,300 kIU/ml), old age (67 years) and sex (female) were poor response factors to the therapy. Low body weight, no alcohol consumption, no coinfection with other viruses, such as hepatitis B virus, and slight fibrosis (F1) were favorable factors for the SVR. Immunological examinations including the percentage of B cells, T cells and the CD4/CD8 ratio were within almost normal limits, except for high natural killer cell activity; consequently, immunologic activity does not explain the SVR in our case.

On-treatment factors are mainly related to viral kinetics within the first few weeks of treatment [25]. A new IRM assay of HCV core antigen is very useful in predicting virological response during PEG-IFN/RBV combination therapy for chronic hepatitis with a high viral load of serum HCV RNA, genotype 1b [26]. Our patient demonstrated a rapid virological decrease in HCV core antigen during 4 weeks after the start of therapy, as revealed by the new IRM assay.

Because the HCV genotype is one of the major factors affecting the response to IFN-based therapy, resistance to IFN is, at least partly, genetically encoded by HCV itself [27]. In this context, nonstructural protein 5A (NS5A), one of the HCV nonstructural proteins, has been widely discussed for its correlation with IFN responsiveness. Sequence variations within a region in NS5A, called 'IFN sensitivity-determining region', have been proposed as correlated with IFN responsiveness [12, 13]. A high degree of sequence variations in the V3 [amino acids (aa) 2356–2379] and the pre-V3 regions (aa 2334–2355) of NS5A, collectively referred to as the 'IFN/RBV resistance-determining region' (aa 2334–2379), is closely correlated with SVR in HCV-1b-infected patients treated with PEG-IFN and RBV [11]. Substitutions of aa

70 (Arg) and 91 (Leu) in the core region (double wild type) are correlated with IFN responsiveness [14]. In our case, only 1 virological factor, the double wild type in the core region, among these 3 virological factors considered to be correlated with SVR, was compatible with SVR.

In conclusion, host factors and viral factors may have contributed to SVR in our case, irrespective of the discontinuation of therapy after 16 weeks. Moreover, acute pancreatitis with high TNF-α might have been related to the SVR. Further study is needed to elucidate the host and viral factors correlated with SVR.

References

1 Yoshizawa H: Trends of hepatitis virus carriers. Hepatol Res 2002;24:S28–S39.
2 Hiramatsu N, Oze T, Tsuda N, Kurashige N, Koga K, Toyama T, Yasumru M, Kanto T, Takehara T, Kasahara A, Kato M, Yoshihara H, Katayama K, Hijioka T, Hagiwara H, Kubota S, Oshita M, Haruna Y, Mita E, Suzuki K, Ishibashi K, Hayashi N: Should aged patients with chronic hepatitis C be treated with interferon and ribavirin combination therapy? Hepatol Res 2006;35:185–189.
3 Charlton MR, Pockros PJ, Harrison SA: Impact of obesity on treatment of chronic hepatitis C. Hepatology 2006;43:1177–1186.
4 McHutchison JG, Gordon SC, Schiff ER, Shiffman ML, Lee WM, Rustgi VK, Goodman ZD, Ling MH, Cort S, Albrecht JK: Interferon alfa-2b alone or in combination with ribavirin as initial treatment for chronic hepatitis C. Hepatitis Interventional Therapy Group. N Engl J Med 1998;339:1485–1492.
5 Poynard T, Marcellin P, Lee SS, Niederau C, Minuk GS, Ideo G, Bain V, Heathcote J, Zeuzem S, Trepo C, Albrecht J: Randomized trial of interferon alpha 2b plus ribavirin for 48 weeks or for 24 weeks versus interferon alpha 2b plus placebo for 48 weeks for treatment of chronic infection with hepatitis C virus. International Hepatitis Interventional Therapy Group. Lancet 1998;352:1426–1432.
6 Manns MP, McHutchison JG, Gordon SC, Rustgi VK, Shiffman M, Reindollar R, Goodman ZD, Koury K, Ling M, Albrecht JK: Peginterferon alfa-2b plus ribavirin compared with interferon alfa-2b plus ribavirin for initial treatment of chronic hepatitis C: a randomized trial. Lancet 2001;358:958–965.
7 Fried MW, Shiffman ML, Reddy KR, Smith C, Marinos G, Gonçales FL Jr, Häussinger D, Diago M, Carosi G, Dhumeaux D, Craxi A, Lin A, Hoffman J, Yu J: Peginterferon alfa-2a plus ribavirin for chronic hepatitis C virus infection. N Engl J Med 2002;347:975–982.
8 Jensen DM, Morgan TR, Marcellin P, Pockros PJ, Reddy KR, Hadziyannis SJ, Ferenci P, Ackrill AM, Willems B: Early identification of HCV genotype 1 patients responding to 24 weeks peginterferon alpha-2a (40 kd)/ribavirin therapy. Hepatology 2006;43:954–960.
9 Eland IA, Rasch MC, Sturkenboom MJ, Bekkering FC, Brouwer JT, Delwaide J, Belaiche J, Houbiers G, Stricker BH: Acute pancreatitis attributed to the use of interferon alfa-2b. Gastroenterology 2000;119:230–233.
10 Chaudhari S, Park J, Anand BS, Pimstone NR, Dieterich DT, Batash S, Bini E: Acute pancreatitis associated with interferon and ribavirin therapy in patients with chronic hepatitis C. Dig Dis Sci 2004;49:1000–1006.
11 El-Shamy A, Nagano-Fujii M, Sasase N, Imoto S, Kim SR, Hotta H: Sequence variation in hepatitis C virus nonstructural protein 5A predicts clinical outcome of pegylated interferon/ribavirin combination therapy. Hepatology 2008;48:38–47.
12 Enomoto N, Sakuma I, Asahina Y, Kurosaki M, Murakami T, Yamamoto C, Izumi N, Marumo M, Sato C: Comparison of full-length sequences of interferon-sensitive and resistant hepatitis C virus 1b: sensitivity to interferon is conferred by amino acid substitutions in the NS5A region. J Clin Invest 1995;96:224–230.
13 Enomoto N, Sakuma I, Asahina Y, Kurosaki M, Murakami T, Yamamoto C, Ogura Y, Izumi N, Marumo F, Sato C: Mutations in the nonstructural protein 5A gene and response to interferon in patients with chronic hepatitis C virus 1b infection. N Engl J Med 1996;334:77–81.
14 Akuta N, Suzuki F, Kawamurua Y, Yatsuji H, Sezaki H, Suzuki Y, Hosaka T, Kobayashi M, Kobayashi M, Arase Y, Ikeda K, Kumada H: Predicative factors of early and sustained responses to peginterferon plus ribavirin combination therapy in Japanese patients infected with hepatitis C virus genotype 1b: amino acid substitutions in the core region and low-density lipoprotein cholesterol levels. J Hepatol 2007;46:403–410.
15 Mallory A, Kern F Jr: Drug-induced pancreatitis: a critical review. Gastroenterology 1980;78:813–820.
16 McArthur KE: Review article: drug-induced pancreatitis. Aliment Pharmacol Ther 1996;10:23–38.
17 Fernández-Miranda C, Castellano G, Guijarro C, Fernández I, Schöebel N, Larumbe S, Gómez-Izquierdo T, del Palacio A: Lipoprotein changes in patients with chronic hepatitis C treated with interferon-alpha. Am J Gastroenterol 1998;93:1901–1904.
18 Naeem M, Bacon BR, Mistry B, Britton RS, Di Bisceglie AM: Changes in serum lipoprotein profile during interferon therapy in chronic hepatitis C. Am J Gastroenterol 2001;96:2468–2472.
19 Shinohara E, Yamashita S, Kihara S, Hirano K, Ishigami M, Arai T, Nozaki S, Kameda-Takemura K, Kawata S, Matsuzawa Y: Interferon alpha induces disorder of lipid metabolism by lowering postheparin lipases and cholesteryl ester transfer protein activities in patients with chronic hepatitis C. Hepatology 1997;25:1502–1506.
20 Steinberg W, Tenner S: Acute pancreatitis. N Engl J Med 1994;330:1198–1210.
21 Russo MW, Fried MW: Side effects of therapy for chronic hepatitis C. Gastroenterology 2003;124:1711–1719.
22 Snell NJ: Ribavirin – current status of a broad spectrum antiviral agent. Expert Opin Pharmacother 2001;2:1317–1324.
23 Malleo G, Mazzon E, Siriwardena AK, Cuzzocrea S: Role of tumor necrosis factor-alpha in acute pancreatitis: from biological basis to clinical evidence. Shock 2007;28:130–140.
24 Zhang XP, Lin Q, Zhou YF: Progress of study on the relationship between mediators of inflammation and apoptosis in acute pancreatitis. Dig Dis Sci 2007;52:1199–1205.
25 Ferenci P: Predictors of response to therapy for chronic hepatitis C. Semin Liver Dis 2004;24:S25–S31.
26 Sasase N, Kim SR, Kim KI, Taniguchi M, Imoto S, Mita K, Hotta H, Shouji I, El-Shamy A, Kawada N, Kudo M, Hayashi Y: Usefulness of a new immunoradiometric assay of HCV core antigen to predict virological response during PEG-IFN/RBV combination therapy for chronic hepatitis with high viral load of serum HCV RNA genotype 1b. Intervirology 2008;51:S70–S75.
27 Welker MW, Hofmann WP, Welsch C, von Wagner M, Herrmann E, Lengauer T, Zeuzem S, Sarrazin C: Correlation of amino acid variations within nonstructural 4B protein with initial viral kinetics during interferon-alpha-based therapy in HCV-1b-infected patients. J Viral Hepatol 2007;14:338–349.

ELSEVIER

Journal of Hepatology 50 (2009) 883–894

Journal of Hepatology

www.elsevier.com/locate/jhep

HCV replication suppresses cellular glucose uptake through down-regulation of cell surface expression of glucose transporters☆

Daisuke Kasai[1,†], Tetsuya Adachi[1,†], Lin Deng[1], Motoko Nagano-Fujii[1], Kiyonao Sada[1], Masanori Ikeda[2], Nobuyuki Kato[2], Yoshi-Hiro Ide[1], Ikuo Shoji[1], Hak Hotta[1,*]

[1]*Divisions of Microbiology, Kobe University Graduate School of Medicine, 7-5-1 Kusunoki-cho, Chuo-ku, Kobe 650-0017, Japan*
[2]*Department of Molecular Biology, Okayama University Graduate School of Medicine and Dentistry, Okayama, Japan*

See Editorial, pages 845–847

***Background/Aims*: Persistent infection with hepatitis C virus (HCV) causes extrahepatic diseases, including diabetes. We investigated the possible effect(s) of HCV replication on cellular glucose uptake and expression of the facilitative glucose transporter (GLUT) 2 and 1.**

***Methods*: We used Huh-7.5 cells harboring either an HCV subgenomic RNA replicon (SGR) or an HCV full-genomic RNA replicon (FGR), HCV-infected cells, and the respective cells treated with interferon (IFN). We also used liver tissue samples obtained from patients with or without HCV infection.**

***Results*: Glucose uptake and surface expression of GLUT2 and GLUT1 were suppressed in SGR, FGR and HCV-infected cells compared to the control cells. Expression levels of GLUT2 mRNA, but not GLUT1 mRNA, were lower in SGR, FGR and HCV-infected cells than in the control. Luciferase reporter assay demonstrated decreased GLUT2 promoter activities in SGR, FGR and HCV-infected cells. IFN treatment restored glucose uptake, GLUT2 surface expression, GLUT2 mRNA expression and GLUT2 promoter activities. Also, GLUT2 expression was reduced in hepatocytes of liver tissues obtained from HCV-infected patients.**

***Conclusions*: HCV replication down-regulates cell surface expression of GLUT2 partly at the transcriptional level, and possibly at the intracellular trafficking level as suggested for GLUT1, thereby lowering glucose uptake by hepatocytes.**

***Keywords*: Diabetes mellitus; Down-regulation; Glucose uptake; GLUT1; GLUT2; Hepatitis C virus; Hepatocyte; Interferon; Replicon**

1. Introduction

Hepatitis C virus (HCV) is a small, enveloped RNA virus, which belongs to the genus *Hepacivirus* within the family *Flaviviridae*. The viral genome consists of single-stranded, positive-sense RNA of 9.6 kb that encodes a polyprotein of about 3000 amino acids. There are six major genotypes of HCV worldwide, with each genotype being further classified into a number of subtypes, such as HCV-1a and -1b [1,2]. The polyprotein is processed by host cellular and viral proteases to yield at least 10 structural and nonstructural (NS) proteins, such

Received 15 June 2008; received in revised form 19 November 2008; accepted 11 December 2008; available online 27 February 2009
Associate Editor: F. Zoulim

☆ The authors who have taken part in the research of this manuscript declared that they do not have a relationship with the manufacturers of the materials involved either in the past or present and they did not receive funding from the manufacturers to carry out their research.

* Corresponding author. Tel.: +81 78 3825500; fax: +81 78 3825519.
E-mail address: hotta@kobe-u.ac.jp (H. Hotta).
† These authors contributed equally to this work.

Abbreviations: FGR, full-genome RNA replicon; GLUT, glucose transporter; HBV, hepatitis B virus; HCV, hepatitis C virus; IFN, interferon; SGR, subgenomic RNA replicon.

0168-8278/$36.00
doi:10.1016/j.jhep.2008.12.029

as core protein, envelope glycoproteins (E1 and E2), p7, NS2, NS3, NS4A, NS4B, NS5A and NS5B [3,4].

HCV prevails in most parts of the world with an estimated number of about 170 million carriers and, hence, HCV infection is a major global healthcare problem [5]. Persistent infection with HCV causes not only liver diseases, including hepatitis, but also extrahepatic manifestations, such as type 2 diabetes [6–8]. While it has been known that liver cirrhosis impairs the glucose metabolism of the liver, there are some reports showing that HCV-infected patients over 40 years old have an increased risk for type 2 diabetes – three times higher than that for patients without HCV infection [9,10]. These reports imply the possibility that HCV infection directly predisposes the host towards type 2 diabetes. However, the precise mechanism(s) is poorly understood.

Glucose is transported into the cell via various isoforms of the facilitative glucose transporter (GLUT) that are present in most cells. Currently, a total of 14 isoforms have been identified in the GLUT family [11–13]. GLUT2 is expressed tissue-specifically in the liver, pancreatic β-cells, hypothalamic glial cells, retina and enterocytes [14]. On the other hand, GLUT1 is expressed at high levels in all fetal tissues and, in adults, it is widely expressed but most abundant in erythrocytes, endothelial cells of the blood–brain barrier, renal tubules of the kidney, and any kind of malignant cells including hepatocellular carcinoma [13].

In the present study, we demonstrated that HCV infection suppressed hepatocytic glucose uptake through down-regulation of surface expression of GLUT in a human hepatocellular carcinoma-derived cell line Huh-7.5. We also demonstrated that GLUT2 expression in hepatocytes of the liver tissues from HCV-infected patients was lower than in those from patients without HCV infection. We propose that HCV replication decreases glucose uptake and cell surface expression of GLUT, which would eventually lead to glucose metabolism disorder.

2. Materials and methods

2.1. Cell culture, HCV RNA replication, HCV infection and IFN treatment

A human hepatoma-derived cell line, Huh-7.5, which is highly permissive to HCV RNA replication [15], was kindly provided by Dr. C.M. Rice (The Rockefeller University, New York, NY, USA). The cells were maintained in Dulbecco's modified Eagle's medium supplemented with 10% heat-inactivated fetal calf serum.

Huh-7.5 cells stably harboring an HCV-1b subgenomic RNA replicon (referred to as SGR cells, hereafter) were prepared as describe previously [16–18], using pFK5B/2884Gly (a kind gift from Dr. R. Bartenschlager, University of Heidelberg, Heidelberg, Germany). In SGR cells, the HCV subgenomic RNA replicon autonomously replicates to express NS3 to NS5B of HCV (Fig. 1). Cells harboring a full-length HCV-1b RNA replicon derived from pON/C-5B (referred to as FGR cells, hereafter) were described previously [19,20]. In FGR cells, the genome-size HCV RNA replicon autonomously replicates to express all the HCV proteins (the core protein, E1, E2, p7, NS2, NS3 to NS5B).

The pFL-J6/JFH1 plasmid that encodes the entire viral genome of a chimeric strain of HCV-2a, J6/JFH1 [21], was kindly provided by Dr. C.M. Rice. The HCV RNA genome was transcribed *in vitro* from pFL-J6/JFH1 and transfected to Huh-7.5 cells. The virus produced in the culture supernatant was used for infection experiments at multiplicities of infection of 1.0 and cultured for 5 days after virus infection.

In some experiments, SGR and FGR cells, as well as HCV-infected cells at 5 days after virus infection, were treated with 1000 IU/ml of IFN (Sigma, St. Louis, MI, USA) for 10 days to eliminate HCV replication.

2.2. Immunofluorescence

Cells were fixed with 3.7% paraformaldehyde and incubated with mouse monoclonal antibody against HCV NS5A (Chemicon International, Inc., Temecula, CA, USA) or HCV core (Abcam, Tokyo, Japan). The cells were then incubated with fluorescein isothiocyanate (FITC)-conjugated goat anti-mouse IgG (MBL Co. Ltd., Nagoya, Japan), and observed under a fluorescent microscope (BX51; Olympus, Tokyo, Japan).

2.3. Immunoblotting

Cells were solubilized in lysis buffer as reported previously [22]. The cell lysates were electrophoresed subjected to 8% polyacrylamide gel electrophoresis and transferred to polyvinylidene difluoride membrane (Millipore Corp., Billerica, MA, USA). The membranes were incubated with mouse monoclonal antibodies against HCV NS5A or NS3 (Chemicon), followed by incubation with peroxidase-conjugated goat anti-mouse IgG (MBL). The positive bands were visualized by using ECL detection system (GE Healthcare UK Ltd., Buckinghamshire, UK).

2.4. Uptake of 2-deoxy-D-glucose and thymidine

Cells cultured in 12-well plates were deprived of serum by incubation in serum-free medium for 12 h. The cells were then pre-incubated for 20 min in 450 μl of KRH (25 mM Hepes, 120 mM NaCl, 5 mM KCl, 1.2 mM $MgSO_4$, 1.3 mM $CaCl_2$, 1.3 mM KH_2PO_4 and 0.1% BSA, pH 7.4). Glucose uptake assay was performed as describe previously [23]. In brief, glucose uptake was initiated by addition of 50 μl of reaction solution (KRH containing 0.5 mM, 0.25 μCi 2-deoxy-D-[1,2-^{3}H]glucose) to each well. As a negative control, 100 μM phloretin was added to reaction solution. After 10 min, transport was terminated by washing the cells with ice-cold KRH buffer containing 100 μM phloretin. The cells were solubilized by 0.1% sodium dodecyl sulfate, and the incorporated radioactivity was measured by liquid scintillation counter (LS6500; Beckman Coulter, Fullerton, CA). In some experiments, GLUT1 and GLUT2 were ectopically expressed by using the pCAGGS expression vector [24] and glucose uptake was measured as described above.

2.5. Flow cytometry

To examine cell surface expression of GLUT1 and GLUT2, cells harvested in PBS containing 0.2% EDTA were incubated with rabbit polyclonal antibodies against GLUT1 or GLUT2 (1:200; Alpha Diagnostic International, San Antonio, TX, USA) on ice for 1 h. After being washed, the cells were incubated with FITC-labeled goat anti-rabbit IgG (1:200; BD Pharmingen, Franklin Lakes, NJ, USA) on ice for another 1 h. Analysis was carried out using flow cytometer and a total of 10,000 live cell events were measured. Results were displayed graphically as overlaying histograms demonstrating the shift of the mean FITC staining value.

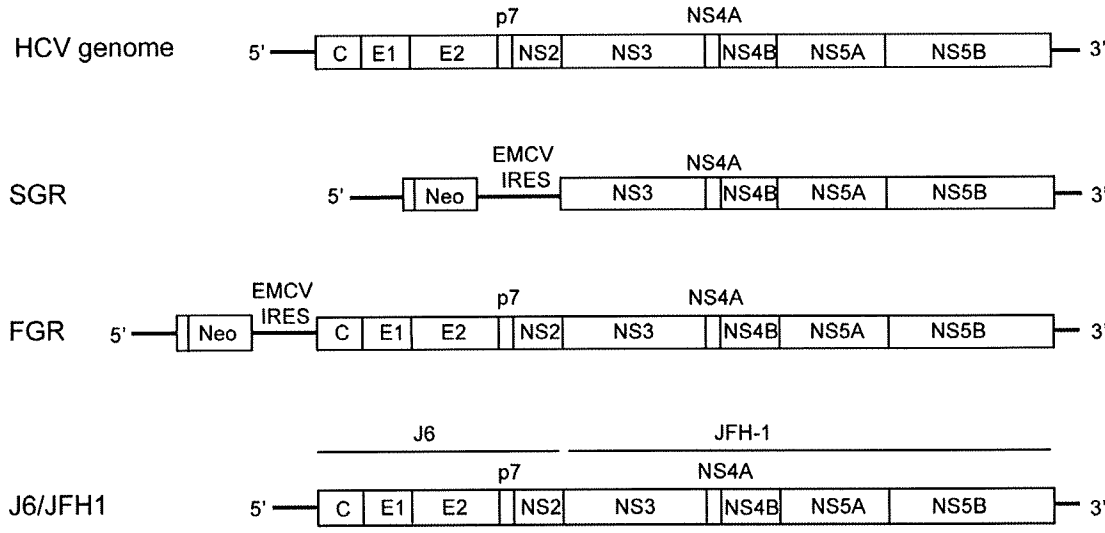

Fig. 1. The HCV genome and HCV RNA replicons. Schematic diagram of the HCV genome, SGR, FGR and the chimeric HCV J6/JFH1 genome are shown. EMCV IRES, encephalomyocarditis virus internal ribosome entry site; Neo, neomycin-resistance gene.

2.6. Real-time quantitative RT-PCR

Total cellular RNA was isolated using the TRIzol reagent (Invitrogen Corp., Carlsbad, CA, USA) and cDNA was generated using QuantiTect Reverse Transcription system (Qiagen, Valencia, CA, USA). Real-time quantitative PCR was performed on a SYBR *Premix Ex Taq* (Takara Bio, Kyoto, Japan) using SYBR green chemistry in ABI PRISM 7000 (Applied Biosystems, Foster, CA, USA). β-Glucuronidase was used as an internal control. The primers used are shown in Table 1.

2.7. Luciferase reporter assay

We constructed the human GLUT2 promoter-luciferase reporter gene (pGLUT2-1291Luc) by cloning a 1.6-kb genomic fragment that encompasses the human GLUT2 promoter (−1291 to +308) [14] into the pGL4 vector plasmid (Promega, Madison, WI, USA). pGLUT2-1291Luc thus contains a 1291-bp fragment of the human GLUT2 promoter upstream of the minimal promoter and the coding sequence of the *Photimus pyralis* (firefly) luciferase. pRL-CMV-*Renilla* (Promega) was used as an internal control. Cells were transfected with pGLUT2-1291Luc (1 μg) and pRL-CMV-*Renilla* (10 ng). After 24 h, a luciferase assay was performed by using Dual-luciferase reporter assay system (Promega). Firefly and *Renilla* luciferase activities were measured by Lumat LB 9501 (Berthold, Bad Wildbad, Germany). Firefly luciferase activity was normalized to *Renilla* luciferase activity for each sample.

2.8. Immunohistochemistry

Human adult liver autopsy materials and surgically removed liver tissues of patients with HCV- or HBV-associated hepatocellular carcinoma, and those with metastatic liver cancer were obtained with written informed consent. The tissues were fixed with 10% buffered formalin (pH 7.0), embedded in paraffin and sectioned at intervals of 4 μm. Immunohistochemical staining was performed with a DAKO ENVISION+ Kit (Dako, Glostrup, Denmark). In brief, fixed sections were treated with 3% hydrogen peroxide, and were autoclaved at 121 °C for 20 min. Then, the sections were incubated with a blocking solution and then with either anti-GLUT2 rabbit polyclonal antibody (Santa Cruz Biotechnology, Santa Cruz, CA, USA) or normal rabbit IgG (Santa Cruz Biotechnology) as a control. The sections were incubated with horseradish peroxidase-labeled polymer-conjugated goat anti-rabbit IgG, followed by incubation in a chromogenic solution. The sections were then counterstained with hematoxylin and examined with a light microscope. GLUT2 expression levels were arbitrarily determined by two examiners, including a pathologist, in a blinded manner.

2.9. Statistical analysis

Results were expressed as mean ± SEM. Statistical significance was evaluated by ANOVA, and statistical significance was defined as $P < 0.05$.

Table 1
Sequences and positions of the primers used in this study.

Gene name (GenBank ID)	Primer	Position	PCR product (bp)
GLUT2	5′-TGGGCTGAGGAAGAGACTGT-3′	279–298	461
(J03810)	5′-AGAGACTGAAGGATGGCTCG-3′	739–720	
GLUT1	5′-TGAACCTGCTGGCCTTC-3′	437–453	399
(AK292791)	5′-GCAGCTTCTTTAGCACA-3′	835–819	
HCV NS5B	5′-ACCAAGCTCAAACTCACTCCA-3′	9191–9211	119
(AJ238799)	5′-AGCGGGGTCGGGCACGAGACA-3′	9309–9289	
β-glucuronidase	5′-ATCAAAAACGCAGAAAATACG-3′	1747–1767	238
(M15182)	5′-ACGCAGGTGGTATCAGTCTTG-3′	1984–1964	

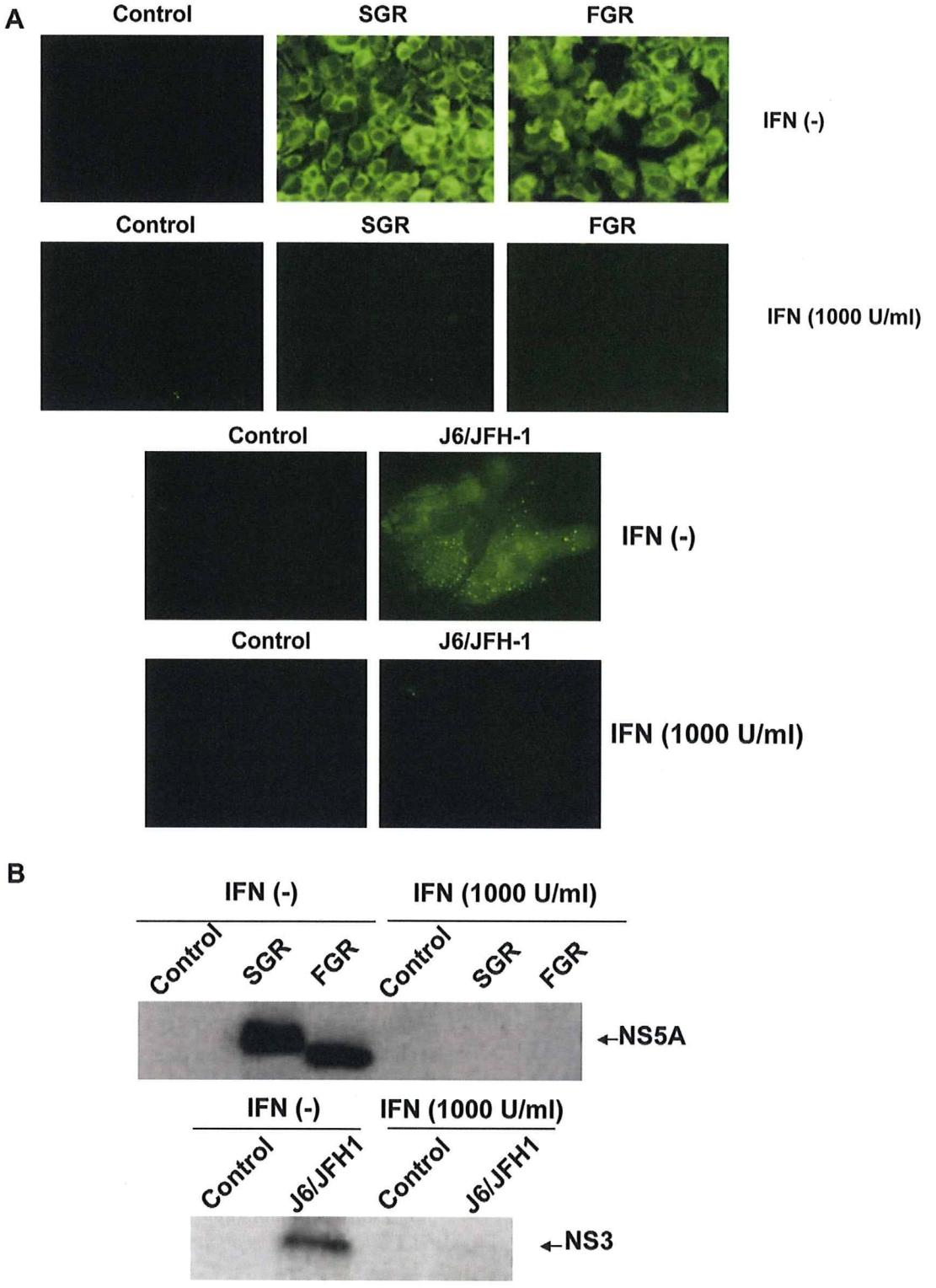

Fig. 2. Expression of HCV proteins in SGR, FGR, HCV-infected cells and the respective cells treated with IFN. (A) Cells were immunostained with anti-NS5A antibody (for SGR, FGR and the control cells) or anti-core antibody (for HCV-infected cells and the control). In parallel, cells were treated with IFN (1000 IU/ml) for 10 days to eliminate HCV replication before being subjected to immunostaining. (B) Cells were analyzed by immunoblotting with anti-NS5A antibody (upper panel) or anti-NS3 antibody (lower panel). In parallel, cells were treated with IFN (1,000 IU/ml) for 10 days to eliminate HCV replication before being subjected to immunoblotting.